


Review

Review on All-Fiber Online Raman Sensor with Hollow Core Microstructured Optical Fiber

Haonan Ding ¹, Dora Juan Juan Hu ² , Xingtao Yu ¹, Xiaoxian Liu ¹, Yifan Zhu ¹ and Guanghui Wang ^{1,*}

¹ College of Engineering and Applied Sciences, Nanjing University, Nanjing 210009, China; mf21340003@smail.nju.edu.cn (H.D.); mf1834023@smail.nju.edu.cn (X.Y.); dg21340008@smail.nju.edu.cn (X.L.); mf20340022@smail.nju.edu.cn (Y.Z.)

² Institute for Infocomm Research, Agency for Science, Technology and Research, Singapore 138632, Singapore; jjhu@i2r.a-star.edu.sg

* Correspondence: wangguanghui@nju.edu.cn

Abstract: Raman spectroscopy is widely used for qualitative and quantitative analysis of trace components in scientific fields such as food safety monitoring, drug testing, environmental monitoring, etc. In addition to its demonstrated advantages of fast response, non-destructive, and non-polluting characteristics, fast online Raman detection is drawing growing attention for development. To achieve this desirable capability, hollow core optical fibers are employed as a common transmission channel for light and fluid in the Raman sensor. By enhancing the interaction process between light and matter, the detection sensitivity is improved. At the same time, the Raman spectroscopy signal light collection efficiency is significantly improved. This article summarizes enhancement techniques reported for Raman sensors, followed by a detailed review on fiber-based Raman sensor techniques including theoretical analyses, fabrication, and application based on hollow core photonic crystal fibers and capillary-based hollow core fibers. The prospects of using these fibers for Raman spectroscopy are discussed.

Keywords: Raman spectroscopy; capillary-based hollow core fibers; hollow core photonic crystal fiber; detection



Citation: Ding, H.; Hu, D.J.J.; Yu, X.; Liu, X.; Zhu, Y.; Wang, G. Review on All-Fiber Online Raman Sensor with Hollow Core Microstructured Optical Fiber. *Photonics* **2022**, *9*, 134. <https://doi.org/10.3390/photonics9030134>

Received: 25 January 2022

Accepted: 23 February 2022

Published: 25 February 2022

Publisher's Note: MDPI stays neutral with regard to jurisdictional claims in published maps and institutional affiliations.



Copyright: © 2022 by the authors. Licensee MDPI, Basel, Switzerland. This article is an open access article distributed under the terms and conditions of the Creative Commons Attribution (CC BY) license (<https://creativecommons.org/licenses/by/4.0/>).

1. Introduction

Rapid detection and identification of chemical substances are of utmost importance in many fields, such as food safety, drug monitoring, industrial wastewater discharging, etc. [1,2]. There are many detection methods which can achieve very accurate qualitative and quantitative detection for their respective application scenarios [3,4]. However, due to the large size of the instrument, the complicated detection process, and the long detection time, these detection methods cannot meet the requirements of fast online detection. Raman spectroscopy is considered as the ‘fingerprint spectrum’ of the matter, which can be used as non-destructive testing and is very suitable for rapid liquid sample testing [5]. However, the Raman signal itself is very weak [6]. This shortcoming limits the application of Raman detection. Much effort has been made to enhance the Raman signal, such as surface-enhanced Raman spectroscopy, tip-enhanced Raman spectroscopy, etc., but these methods are not suitable for fast detection. Moreover, multiple tests cannot be performed, which leads to cross-contamination of the sample, and any impurities can seriously affect the Raman scattering signal. The detection range is concentrated on the focal position of the excitation light, and the interaction volume between the light and the sample is small.

The hollow core fiber (HCF) can confine the excitation light and the Raman signal in the cavity to propagate at the same time. Through internal multiple reflections, the optical path is lengthened, thereby increasing the volume of interaction between the light and the sample and increasing the intensity of the Raman signal. At the same time, within the fiber-enhanced Raman spectroscopy (FERS) structure, the diameter of the HCF used can

reach hundreds of microns, which can perform liquid exchange faster, so as to achieve rapid switching of test samples, which is more suitable for rapid test scenarios.

This paper presents a review of all-fiber online Raman sensors with hollow core microstructured optical fibers. Firstly, the principle of Raman spectroscopy and the methods for Raman signal enhancement are introduced in Section 2. Secondly, based on the overview of Raman sensors with field enhancements, FERS is introduced with different types of commonly used hollow core microstructured optical fibers in Section 3. The hollow core can be used to guide light and sample flow simultaneously. Based on its enhancement of interaction length, in Section 4, we theoretically analyze its enhancement mechanism. Moreover, several in-fiber optical path modification methods are proposed to further enhance the interaction length. Then, in Sections 5 and 6, we present a comprehensive review of their applications in detail, focusing on hollow core photonic crystal fiber and capillary-based hollow core fiber, respectively. In total, four kinds of optical fibers are discussed and their applications are summarized. In Section 7, from the perspective of testing samples, we also summarize the application cases of fiber-enhanced Raman sensors. Finally, the prospects of using these hollow core microstructured optical fibers in Raman spectroscopy are summarized and concluded.

2. Principle of Raman Spectroscopy and Overview of Raman Sensor with Enhancement

2.1. Principle of Raman Spectroscopy

In 1928, Indian scientist C. V. Raman discovered a new scattering effect, known as the Raman effect, when studying the liquid scattering of monochromatic light by a mercury lamp [7]. The effect explains the wavelength shift of scattered light from a small fraction of the molecules, which has a frequency different from that of the incident light, depending on the chemical structure of the corresponding molecule. Raman spectroscopy uses scattered light to obtain information about molecular vibration, which can provide specific information about structure, symmetry, molecular bonding, electronic environment, etc. [8]. Therefore, Raman spectroscopy can be applied to qualitative and quantitative analysis of various compounds.

When light with a frequency interacts with matter, inelastic scattering will occur. The wavelength of the scattered light of a small part of the molecule is shifted, and the photon obtains vibration energy from the molecule. The energy of the scattered light is increased and is called anti-Stokes Raman scattering, and on the contrary, the energy of the scattered light is reduced to Stokes Raman scattering [9]. The energy level diagram is shown in Figure 1. Since most of the molecules are in the ground state at room temperature, it can be seen from the Boltzmann distribution that the Stokes scattering is much stronger than the anti-Stokes scattering. Therefore, the Stokes scattering spectrum is usually used when studying Raman scattering spectra. Raman spectroscopy uses scattered light to obtain information about molecular vibration. As the vibrations of material molecules are different, the Raman spectra are also different, so Raman spectroscopy is also called the ‘fingerprint spectrum’ of the object [5]. Using this characteristic of Raman spectroscopy, the composition and concentration of the sample can be distinguished, and the qualitative and quantitative analysis of the sample can be realized.

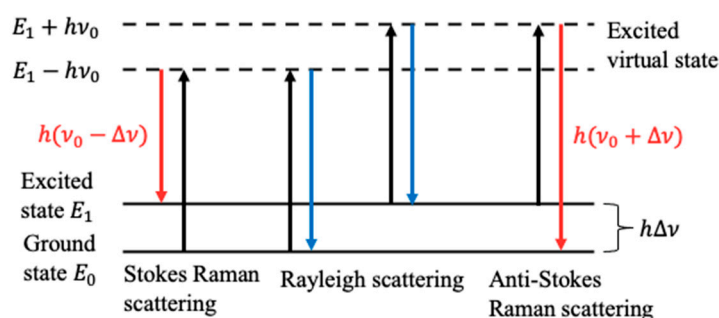


Figure 1. Rayleigh scattering and Raman scattering energy level diagram. Reproduced with permission [10].

2.2. Overview of Raman Sensor with Enhancement

As the Raman scattering signal is very weak, in recent years, many researchers have devoted themselves to researching methods to enhance the Raman signal with great progress. They proposed enhancement methods include resonance Raman spectroscopy (RRS), coherent anti-Stokes Raman spectroscopy (CARS) [11], cavity-enhanced Raman spectroscopy (CERS) [12], surface-enhanced Raman spectroscopy (SERS) [13], fiber-enhanced Raman spectroscopy (FERS), etc.

Resonance Raman spectroscopy (RRS): In the 1950s, Shorygin et al. proposed that when the excitation photon energy roughly matches the energy required for the electron transition in the sample, the measured Raman spectrum intensity will increase significantly. This method is called RRS, which can detect the Raman spectra of samples with concentrations as low as 10^{-8} mol/L. RRS has been widely used in the analysis of various luminescent biological samples, such as enzymes. The excitation light can be adjusted to the specific absorption band of the active part of the enzyme. Therefore, RRS can selectively determine its structure [14]. In addition, using different wavelengths of excitation light, the vibrational spectra of various parts of biomolecules can be obtained [15].

Coherent anti-Stokes Raman spectroscopy (CARS): In 1965, Maker et al. [16] first reported the ‘three-wave mixing experiment’. In 1974, Begley et al. [11] called it CARS. This technology realizes vibration imaging with high sensitivity, high spectral resolution, and a three-dimensional slice function. CARS is a non-linear detection technology based on inducing coherent Raman on the target molecule. Two lasers are detected by the third laser, and a coherent signal with a blue shift of frequency is generated in the direction of phase matching. CARS is an effective method to measure the temperature and main component concentration in the reaction fluid [17], and it can detect different molecular bonds in various biological systems. CARS based on nanosecond, picosecond, and femtosecond lasers also has a wide range of applications in gas-phase reaction streams [18].

Cavity-enhanced Raman spectroscopy (CERS): Since the Raman signal and laser power are linear, the problem of low sensitivity of spontaneous Raman scattering can be solved by using a higher power laser. One method is to place the Raman cavity and the gain medium together in the laser resonator, so as to utilize the efficient laser power in the laser resonator (in-cavity laser Raman spectrometer) [12]. Another method is to use the laser power accumulated in the external optical cavity. Its simplest form is composed of two highly reflective mirrors with two parallel sides. If the laser frequency is stabilized at the resonant frequency of the cavity, then light can be efficiently coupled into the cavity, and the laser power can be enhanced by several orders of magnitude. This kind of power accumulation in an optical cavity can be used to improve the efficiency of spontaneous Raman scattering, which is called CERS [19]. In 2001, Taylor et al. [20] realized the specific application of CERS for the first time. Through the electronic feedback mechanism, the 1 W, 532 nm laser was stabilized in a short linear cavity, and the Raman cavity was placed in the optical cavity. The Raman signal of hydrogen is detected from the 90° direction, but the Raman cavity window causes a lot of optical loss, resulting in the enhancement factor being limited to about 50 times.

Surface-enhanced Raman spectroscopy (SERS): In 1974, Fleischmann et al. [13] discovered the phenomenon of SERS. SERS can be used to detect and identify very low-concentration molecular species. This method is based on adsorbing the analyte to the surface of a metal structure, usually gold, silver, or copper, and mainly uses the local electromagnetic field generated by the assembly of nanostructured materials and the strong field enhancement generated by the electromagnetic coupling between the nanoparticles, which overcomes the obstacle of small scattering cross-section [21]. Compared with normal Raman scattering, the Raman scattering cross-section of the analyte in the SERS detection method is increased by up to 15 orders of magnitude, and the Raman signal of the target molecule is also increased by several orders of magnitude, so that SERS can even detect the Raman signal of a single molecule. In recent years, in order to improve the stability and reproducibility of SERS substrates, and to further increase the enhancement rate of SERS, metal nanoresonators with more controllable shapes and reproducible shapes have been introduced on solid substrates, such as a metal film on a nanosphere substrate and metal-coated alumina nanoparticles.

Tip-enhanced Raman spectroscopy (TERS): Like other pure optical techniques, the spatial resolution of standard SERS measurements is limited by the Abbe diffraction limit $\lambda/2$, where λ is the wavelength of the incident radiation. However, this diffraction limit may be overcome. In 2000, Zenobi et al. [22] showed that it is possible to couple Raman spectroscopy with scanning tunneling microscopes or atomic force microscopes to form a new spectral microscope tool, the so-called tip-enhanced Raman spectroscopy. In TERS detection, the sharp AFM (or STM) tip made of SERS active metal is moved toward the sample to be tested and irradiated with a laser [23], and the Raman scattering generated by the sample under the tip is enhanced. Neacsu et al. [24] achieved the tip-induced Raman scattering enhancement in the experiment, reaching 5×10^9 . In this way, TERS can detect Raman spectra with high spatial resolution. The TERS detection method is relatively complicated. The current research of TERS aims to improve the sensitivity of detection, such as detecting the Raman signal of a single molecule.

Fiber-enhanced Raman spectroscopy (FERS): Compared with normal Raman scattering, the Raman signal enhancement multiples obtained by SERS, TERS, CERS, and other methods are as high as ten orders of magnitude, but in most cases, the volume of light-object interaction is very small, and the volume is proportional to the intensity of the Raman signal. In addition, the molecules adsorbed on the metal surface are difficult to clean, and any tiny impurities or pollution on the metal surface will significantly affect the Raman signal [25,26], so these methods are not suitable for online detection that needs to be reused. Therefore, this article mainly introduces the method of FERS. The Raman scattering spectrum of the sample is detected by injecting the sample into the HCF. This method is simple to use and is suitable for online rapid Raman detection. FERS is discussed in detail in subsequent sections.

3. Fiber-Enhanced Raman Spectroscopy (FERS)

FERS is based on confining light and substances in the hollow core channel of the HCF. On one hand, the sample and the excitation light can be fully used, and on the other hand, the fiber can enhance the Raman light collection effect, enhancing the Raman signal [27]. Traditional waveguide transmission is based on total internal reflection, requiring the core layer to have a higher refractive index than the cladding layer. However, for HCF, the core layer is air, and the refractive index is lower than that of the cladding layer, which cannot meet the condition of total internal reflection. Therefore, other methods are needed to realize the hollow core waveguide, such as leveraging the photonic band gap effect or anti-resonance to achieve hollow core guidance, or forming a liquid core with a higher refractive index than cladding to achieve total internal reflection, coating a highly reflective metal layer on the inner wall or hollow core photonic crystal fiber, etc., so that light can be transmitted in the hollow core. According to specific applications, the current

studies on FERS are mainly divided into hollow core photonic crystal fibers (HCPCFs) and capillary-based HCFs.

3.1. Hollow Core Photonic Crystal Fiber (HCPCF)

HCPCF is a special type of microstructured optical fiber. The current applications in Raman detection mainly include two types of HCPCF, hollow core photonic band gap fiber (HCPBGF) and hollow core anti-resonant photonic crystal fiber (HCARF). HCPCF has the characteristics of hollow structure, small dispersion, small non-linear coefficient, and low transmission loss. It has important application value and broad application prospects in the interaction of light and gas, high-energy laser transmission, pulse compression, optical fiber sensing, and next-generation optical communications [28].

For HCPBGF, several capillaries are removed in the center to form the hollow core, and the surrounding capillaries are arranged in a honeycomb structure to form a cladding, as shown in Figure 2a. For the HCAREF, the cladding can be composed of several non-contact thin-walled capillaries, and the beam is confined in the core by enhancing the reflection of the incident light when it meets the thin wall of the cladding, as shown in Figure 2b.

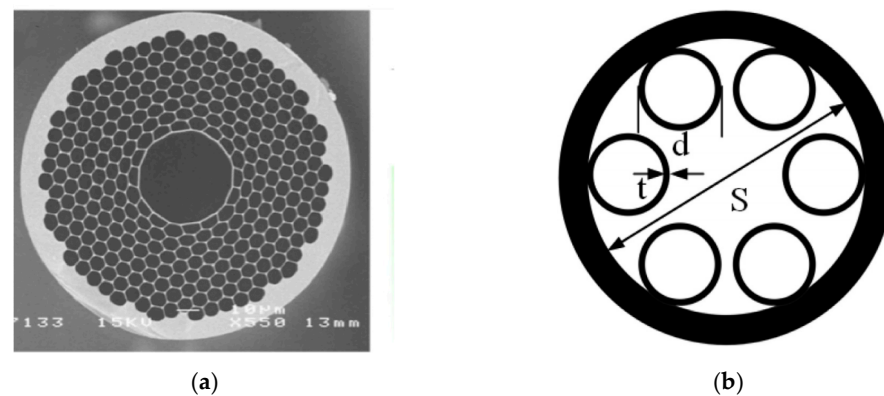


Figure 2. (a) Cross-section of HCPBGF. Reprinted with permission from [29]; © The Optical Society. (b) Cross-section of HCAREF. Reprinted from [30], copyright (2019), with permission from Elsevier.

3.2. Capillary-Based Hollow Core Fiber (HCF)

Compared with HCPCF, capillary-based HCF has a large hollow core aperture, which can increase the volume of light and confine the light while realizing rapid switching of the sample, without requiring a large pressure to inject the sample. Capillary-based HCFs have two main categories, namely metal-lined hollow core fiber (MLHCF) and liquid core fiber (LOF).

For MLHCF, the inner wall of the glass capillary tube is plated with metal to increase the reflectivity to ensure the transmission of light in the core. Due to the high reflectivity of the metal, the Raman signal can be bound in the capillary core to improve the signal collection efficiency. In addition, the inner diameter of the inner aluminized capillary tube is large, liquid can be injected directly under normal pressure, and cross-contamination is small when changing the sample, which is suitable for fast and convenient online detection. The hollow core aperture of the MLHCF is generally several hundred microns. The sample is injected into the fiber, the excitation light emitted by the laser is coupled into the hollow core from one end of the inner MLHCF and is bound in the capillary under the action of the metal layer [31], and the light interacts with the sample to generate Raman light. A part of the Raman scattered light continues to propagate forward, and a part is reflected back to the incident end [32,33]. Therefore, the receiving end of the Raman signal can be divided into transmission Raman detection and reflection Raman detection.

For LOF, its discovery originated in the mid-19th century, when people first conducted scientific research on light guidance in liquids. It was not until 1970 that scientists began to use LOFs as potential communication media [34,35]. The liquid core fiber is composed of a small-diameter glass tube filled with high refractive index liquid, and has low loss in the near-infrared band [34,36], which has obvious practical significance. Compared with traditional experimental equipment, LOF has great advantages in analog communication [37]. In spontaneous Raman spectroscopy, by limiting the excitation radiation and effectively collecting Raman scattered light with a long interaction length, the liquid core fiber can produce an enhancement factor that is 1000–3000 times higher than that of the traditional fiber [38]. There are also huge advantages in the application of absorption spectroscopy [39] and fluorescence spectroscopy [40].

In addition to the enhancement based on HCPCF and HCF, further enhancement can be achieved by introducing optical path configurations, such as a Sagnac loop, capillary with an inserted reflector, and capillary with an inserted FP cavity. The theoretical part of the enhancement by the optical path configuration will be explained in Section 4.2, and the experiment will be shown in Section 6.1.2.

4. Theoretical Analysis

4.1. Theoretical Analysis of FERS

The signal enhancement is mainly caused by the increased interaction length between confined light and samples in the HCF, which provides high-efficiency Raman signal collection. The Raman scattering signal can be described by the equation [41]:

$$P \propto m\sigma V I_0 (\nu_0 - \nu_r)^4. \tag{1}$$

In Equation (1), m is the number of molecules per unit volume, σ is the Raman scattering cross-section of each molecule, V is the sample volume that is irradiated by the pump light, and the scattered light can be received. I_0 , ν_0 , and ν_r are the intensity of the excitation light, Raman light frequency, and excitation light frequency, respectively. The enhancement of the Raman signal can be obtained by increasing the intensity of excitation light including selecting a high-power laser and optical focusing. However, the former easily causes optical loss and thermal effect. Additionally, the latter reduces the volume of the light object while increasing the intensity of light, which is only applicable to the case of limited sample volume [42].

When the laser power is constant P_p , if the power distribution of the excitation light on the sample is uniform, the light intensity can be expressed as P_p/S , where S is the cross-sectional area of the sample, L is the optical path length, and the volume can be expressed as SL . Hence, the increase in optical path length could enhance the Raman light.

Another key consideration in increasing the Raman signal is the collection efficiency of the signal. As shown in Figure 3a, in the case of beam focusing, only the Raman light at the focal point in the lens numerical aperture (NA) can be accepted, and the collection efficiency is $\eta = S_{\text{focus}} \cdot h \cdot \Omega_{\text{obj}} / 4\pi$. For the case of introducing the HCF, as shown in Figure 3b, the HCF can collect the Raman signal in the entire hollow core, which is a large-volume signal. This enhancement mechanism is called volume-enhanced Raman scattering. At this time, the collection efficiency is $\eta = 1/2 \cdot SL \cdot \min(\Omega_{\text{obj}} / \Omega_{\text{HCF}}, 1)$. Ω_{obj} and Ω_{HCF} are the solid angles corresponding to the NA of the lens and the HCF, respectively. For the focusing structure, only the samples in the excitation light focus volume $S_{\text{focus}} \cdot h$ can be excited by the excitation laser in the optical path to generate Raman signal (S_{focus} is the focal area and h is the depth of focus). In addition, the Raman scattered light diverges uniformly in all directions, and only the Raman light within the solid angle $\Omega_{\text{obj}} / 4\pi$ corresponding to the NA can be received by the lens. Compared with the lens, HCF is more advantageous because of the large NA and the capacity for confining the Raman light within the entire fiber. At the output end, if the NA of the lens is smaller than that of the HCF, then the Raman optical coupling efficiency is $\Omega_{\text{obj}} / \Omega_{\text{HCF}}$.

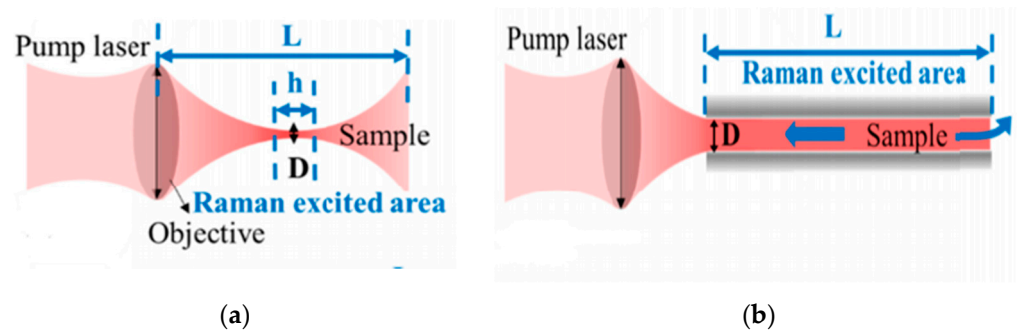


Figure 3. (a) The excitation light is focused on the object. (b) The excitation light is coupled into the HCF and has a long acting distance. Reprinted with permission from [43] © The Optical Society.

4.2. Theoretical Calculation of Raman Signal Enhancement

Through theoretical calculations, the Raman signal strength can be estimated. Here, we mainly discuss the calculation of Raman signal intensities in direct detection and the structure with MLHCF.

In the case of direct detection by the Raman probe, only the Raman light within the focal volume of the probe lens can be received by the probe. The focus volumes of different lenses are different, but the focus volume is very small compared to the hollow core volume of the MLHCF. The Raman signal intensity P_{probe} in the direct detection structure can be expressed by Equation (2), the focal volume can be equivalent to a cylinder, and h is the focal depth of the lens. S_{focus} is the cross-sectional area of the focus volume and $\eta_{probe} = \Omega_{obj}/4\pi$ is the receiving efficiency of the lens. Since the Raman light diverges in all directions, only the Raman light within the solid angle corresponding to the NA of the lens can be received by the probe.

$$P_{Probe} = \int_0^h \sigma m S_{focus} \eta_{probe} I_0 \exp(-\kappa_1 l) \exp(-\kappa_2 l) dl \tag{2}$$

In the case of using the structure with MLHCF, gold and silver have high reflectance for both 785 nm excitation light and its Raman light, so the MLHCF with gold or silver inside can effectively confine the light. As shown in Figure 4b, the Raman probe is coupled with the MLHCF through the optical fiber. The Raman light in the HCF with the same transmission direction as the excitation light is called transmitted Raman light, and the Raman signal propagating in the opposite direction is called reflected Raman light. Our research group selected the Raman spectrometer from Bidatek, and the structure of the Raman probe is shown in Figure 4a. The excitation light is irradiated onto the sample through the band-pass filter, dichroic mirror, and lens. If the excited Raman light is within the NA angle of the lens, it will be received by the lens, and will enter the receiving fiber through the dichroic mirror, mirror, and long-pass filter for Raman signal analysis. Band-pass filters and dichroic mirrors are used to prevent excitation light from entering the excitation fiber and damaging the laser. The long-pass filter is used to prevent the stronger excitation light from entering the receiving fiber.

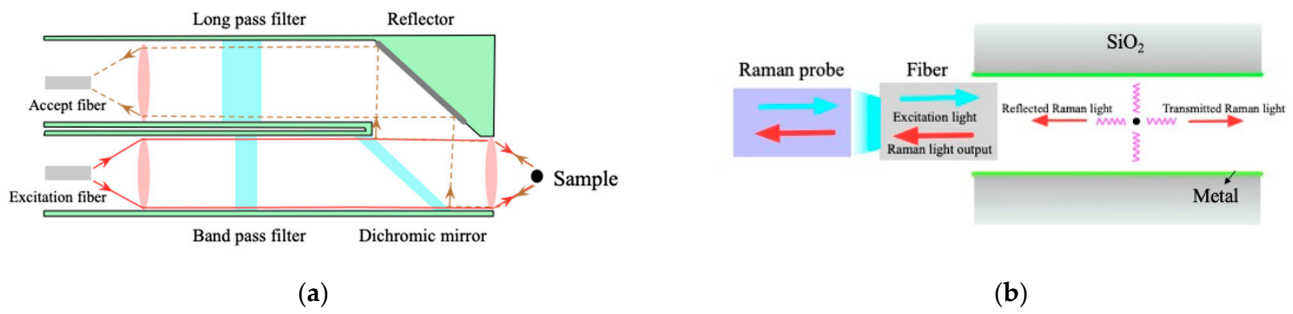


Figure 4. (a) Internal structure diagram of Bidatek Raman probe. (b) Detection principle diagram of MLHCF. Reproduced with permission [10].

When the excitation light is transmitted from the optical fiber to a position with a distance l from the optical fiber, the excitation light intensity I will be attenuated to $I * \exp(-\kappa_1 l)$. The reflected Raman light excited here will be attenuated to $I * \exp(-\kappa_1 l) * \exp(-\kappa_2 l)$. Considering that only the Raman light irradiated within the core diameter of the optical fiber and within its maximum receiving angle range can be received by the optical fiber, the receiving efficiency is $\eta = (d/D)^2 * (2\pi(1 - \cos \alpha)/4\pi) * (\Omega_{obj}/\Omega_{fiber})$, where d is the fiber core diameter, D is the inner diameter of the HCF, α is the maximum acceptance angle of the fiber, Ω_{fiber} and Ω_{obj} are the solid angles corresponding to the NA of the lens and the fiber, respectively. The intensity of the reflected Raman signal and transmitted Raman signal received by the Raman probe in the structure of Figure 4b can be expressed by Equations (3) and (4). Compared with the direct detection, the Raman signal can be significantly enhanced by using the structure with MLHCF.

$$P_R = \int_0^L \sigma m \pi \left(\frac{D}{2}\right)^2 \eta I_0 \exp(-\kappa_1 l) \exp(-\kappa_2 l) dl \tag{3}$$

$$P_T = \int_0^L \sigma m \pi \left(\frac{D}{2}\right)^2 \eta I_0 \exp(-\kappa_1 l) \exp[-\kappa_2(2L - l)] dl \tag{4}$$

Besides using MLHCF, there other structures which are used to enhance the interaction length of light objects and the efficiency of collecting Raman light, including a Sagnac loop, capillary with an inserted reflector, and capillary with an inserted FP cavity.

4.2.1. Sagnac Loop

As shown in Figure 5, the Sagnac loop allows the excitation light to enter and exit from both ends of the HCF simultaneously. In this way, both the transmitted Raman light and the reflected Raman light can be collected. The Raman light can be divided into four parts: the transmission and reflection Raman signals generated by the excitation of the two ends, respectively. The reflected Raman signal and the transmitted Raman signal output by the excitation light I_1 generated by the optical fiber 1 are:

$$P_R(L, I_1) = \sigma m \pi \left(\frac{D}{2}\right)^2 \eta I_1 \int_0^L \exp(-\kappa_1 l) \exp(-\kappa_2 l) dl, \tag{5}$$

$$P_T(L, I_1) = \sigma m \pi \left(\frac{D}{2}\right)^2 \eta I_1 \int_0^L \exp(-\kappa_1 l) \exp[-\kappa_2(L - l)] dl. \tag{6}$$

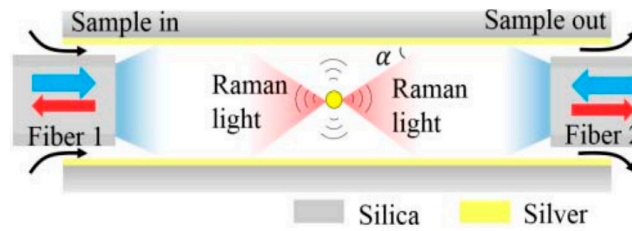


Figure 5. Diagram of light propagation in the Sagnac loop. © (2018) IEEE. Reprinted, with permission, from [32].

In the same way, $P_R(L, I_2)$ and $P_T(L, I_2)$ can be obtained, so the total Raman optical signal is:

$$P_{total}(L, I_1, I_1) = P_R(L, I_1) + P_T(L, I_1) + P_R(L, I_2) + P_T(L, I_2). \quad (7)$$

Comparing the intensity of Raman detection before and after adding Fiber 2 to the end, the Raman enhancement ratio of the structure of the Sagnac loop is:

$$\gamma = \frac{P_{total}}{P_R(L, I_1)}. \quad (8)$$

Jin et al. reported that the Raman enhancement ratio of the structure is about four times [44], which confirms that the all-fiber detection system with a Sagnac loop is a very effective way to enhance the Raman signal.

4.2.2. Capillary with an Inserted Reflector

In the capillary with an inserted reflector structure, a metal reflective film is placed on the other port opposite the laser in the HCF which can reflect the excitation light and Raman light back to the probe, thereby increasing the distance of the light object and the Raman light receiving efficiency. In this structure, the Raman signal is also divided into four parts as Figure 6 shows, the reflected Raman light intensity P_1 and the transmitted Raman light intensity P_2 generated by the excitation light transmitted to the HCF. After passing through the cavity again, the reflected Raman light intensity P_3 and the transmitted Raman light intensity P_4 are generated. The formulas are as follows:

$$P_1 = \sigma m \pi \left(\frac{D}{2}\right)^2 \eta I_0 \int_0^L \exp(-\kappa_1 l) \exp(-\kappa_2 l) dl, \quad (9)$$

$$P_2 = \sigma m \pi \left(\frac{D}{2}\right)^2 \eta I_0 R \left(\frac{d}{D}\right)^2 \int_0^L \exp[-\kappa_1(2L - l)] \exp(-\kappa_2 l) dl, \quad (10)$$

$$P_3 = \sigma m \pi \left(\frac{D}{2}\right)^2 \eta I_0 R \left(\frac{d}{D}\right)^2 \int_0^L \exp(-\kappa_1 l) \exp[-\kappa_2(2L - l)] dl, \quad (11)$$

$$P_4 = \sigma m \pi \left(\frac{D}{2}\right)^2 \eta I_0 R \left(\frac{d}{D}\right)^4 \int_0^L \exp[-\kappa_1(2L - l)] \exp[-\kappa_2(2L - l)] dl. \quad (12)$$

Therefore, the total light intensity is:

$$P_{total} = P_1 + P_2 + P_3 + P_4. \quad (13)$$

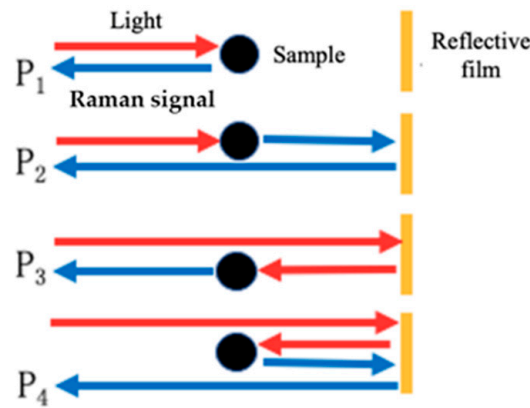


Figure 6. Raman signal transmission diagram in the capillary with an inserted reflector.

The enhancement by the inserted reflector is P_{total}/P_1 in comparison with a structure without the inserted reflector. Chu et al. reported the enhanced Raman signal to be around 1.73 times using the capillary with an inserted gold surface reflector [45].

4.2.3. Capillary with an Inserted FP Cavity

In the capillary with an inserted FP cavity structure, a long-pass filter and a metal reflector are introduced on both sides of the HCF cavity to confine the excitation light to reflect back and forth in the cavity until the light intensity attenuates to zero, as shown in Figure 7. It can be seen that the expression of light intensity is an infinite series, and we calculate the sum of it and obtain the light intensity at position x in the cavity as:

$$I_e(x,l) = \frac{I_1(x) + I_2(x,l)}{1 - R_1R_2e^{-2\alpha l}} \tag{14}$$

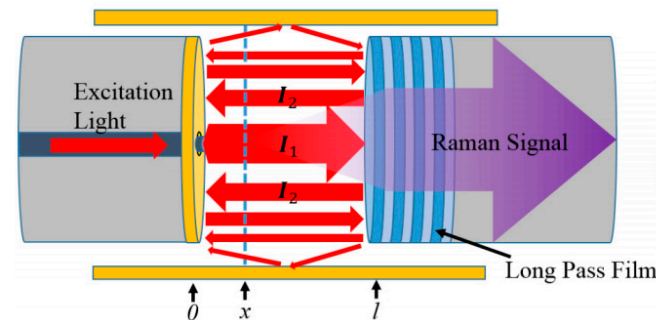


Figure 7. Schematic diagram of excitation light reflecting back and forth in the cavity, while the total light intensity is their scalar summation. Reprinted with permission from [46] © The Optical Society.

From the calculation formula of the Raman signal, the Raman signal can be obtained as:

$$P = \sigma m \pi \left(\frac{D}{2}\right)^2 \eta \int_0^l \left[e^{-\alpha(l-x)} + e^{-\alpha(l+x)} \right] I_e(x,l) dx. \tag{15}$$

Yu et al. reported that in the comparison with the structure without an inserted FP cavity, the enhancement ratio can reach about five times [46]. Here, we list the enhancement ratios of the three structures above in Table 1, and the specific experiment details will be described in Section 6.1.2.

Table 1. Comparison of the enhancement ratios of three different optical path configurations.

	Sagnac Loop	Capillary with an Inserted Reflector	Capillary with an Inserted FP Cavity
Enhancement Ratio	4 [44]	1.73 [45]	5 [46]

5. Photonic Crystal Fiber for Raman Sensing

5.1. Hollow Core Photonic Band Gap Fibers (HCPBGFs)

For HCPBGF, several capillaries are removed in the center, and the surrounding capillaries are arranged in a honeycomb structure to form a cladding [47]. The cladding is composed of SiO₂ and periodic arrangement of air holes. The transmission characteristics depend on the shape, size, and arrangement of air holes in the cladding. Different structures result in different photonic band gaps. When the light wave is incident on the core-cladding interface, the light wave is strongly scattered by periodic air holes in the cladding, and the light wave with specific wavelength satisfying the Bragg condition will return to the core by the photonic band gap effect [48]. Therefore, HCPBGF has strong wavelength selectivity for light transmission [49]. Only the light within the band gap can be transmitted, and the light beyond the band gap will leak into the cladding and redistribute in the cladding. Therefore, when designing the Raman experiment, it is necessary to design the structure of HCPBGF according to the Raman frequency shift range of the detected sample, so that the excitation light and Raman light are in the band gap of the fiber, so as to realize the desirable transmission of the signal. Only in this way can we strengthen the control of the excitation light and Raman light, and increase the interaction between light and matter.

The transmission loss of HCPBGF is very low for sensing applications, e.g., 1 dB/km [50], and the diameter of a hollow core hole is usually 5–30 μm. NA of HCPBGF is 0.2 [9], allowing transmission of a high-intensity laser in the hollow core for a long distance and collection of a strong Raman signal, with the enhancement factor being up to three orders of magnitude. Therefore, HCPBGF is very suitable for applications requiring high sensitivity and a low detection limit.

The band gap range of an HCPBGF is related to factors such as air filling ratio, effective refractive index, and air hole spacing. Based on the expression for the longitudinal wave vector of the light wave, $k_a = \frac{2\pi a}{\lambda}$ [51], where a is the aperture of the air hole, it can be seen that the shorter the wavelength, the smaller the aperture of the air hole that is needed. In other words, the photonic band gap period becomes smaller. At present, the wavelength in the photonic band gap of most HCPCFs is limited to the infrared communication band (0.85–1.55 μm). Due to the small wavelength of the visible light band, the microstructure size of the optical fiber needs to be greatly reduced compared with the transmission of infrared wave band light waves [52], which brings a certain degree of difficulty to the preparation of the optical fiber.

When the HCPBGF is filled non-selectively with liquid in all the air holes, the band gap of the photonic crystal fiber will move to a shorter wavelength due to the change in the refractive index of the cladding and the core, and the spectral width of the band gap will be narrow due to the decrease in the dielectric contrast, which limits the selection of the excitation wavelength and the available range of the Raman spectrum. In order to solve the problem of band gap narrowing caused by non-selective filling, it is necessary to selectively fill the photonic crystal fiber, that is, only the sample enters the hollow core hole, and the air holes in the cladding are not filled. One method is to use polymer to block the air holes of the cladding, but polymer will produce a strong fluorescence background, so this method is not suitable for FERS. Another method is to heat the cladding honeycomb structure to make it collapse, while the hollow core with bigger pore size remains hollow, so that only the sample is passed into the core, as shown in Figure 8. In this case, the HCPBGF can realize light transmission by total internal reflection in the whole visible and near-infrared spectrum range [53]. This novel fiber-enhanced method is used for the detection of the commonly used broad-spectrum antibiotic moxifloxacin, in which only 4 nL of sample

is required, and the detection limit is as low as 1.7 μM , making it possible to detect the concentration of antibiotics in serum or other body fluids without damage and with high sensitivity and rapid detection.

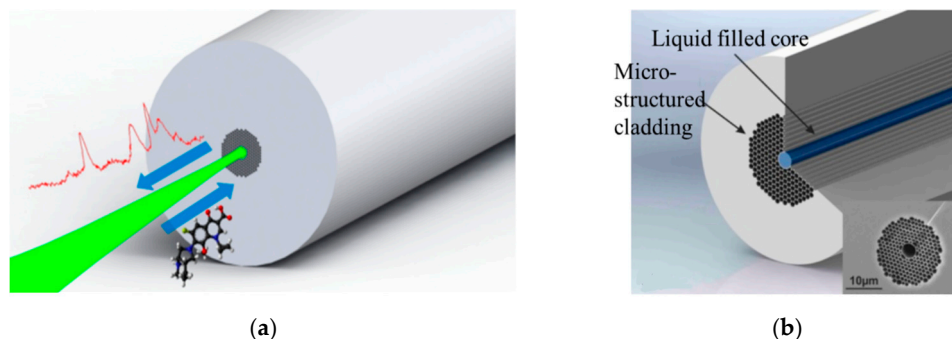


Figure 8. Raman detection principle diagram of hollow core photonic crystal fiber. (a) Raman light is generated by the interaction between the substance and the laser in the HCPCF. The green represents the laser transmitted in the central hole, and the red represents the Raman spectrum. (b) A cross-sectional view of a hollow core photonic crystal fiber selectively filled with a central hole. Reprinted with permission from [53]. Copyright (2017) American Chemical Society.

There are two kinds of loss in HCPBGF: limiting loss and scattering loss [54]. The limiting loss refers to the optical loss caused by the leakage of some conducted light from the cladding during transmission. The limiting loss can be reduced by increasing the number of air holes in the cladding [55]. Scattering loss refers to the loss due to surface roughness induced by surface capillary wave inevitably due to thermodynamic reasons during the pulling of HCPBGF. The core wall can be designed to reduce the roughness of the inner wall to reduce the scattering loss [56]. The lowest reported loss of HCPBGF is about 1 dB/km [50]. Hanf et al. measured the Raman spectrum of H_2 in the HCPBGF, with the equipment as shown in Figure 9a, and studied the influence of different hollow core apertures (Figure 9b) on noise and SNR, and the result is shown in Figure 9c. The result shows that in a certain range, the larger the pinhole size is, the greater the noise is and the smaller the SNR is [57].

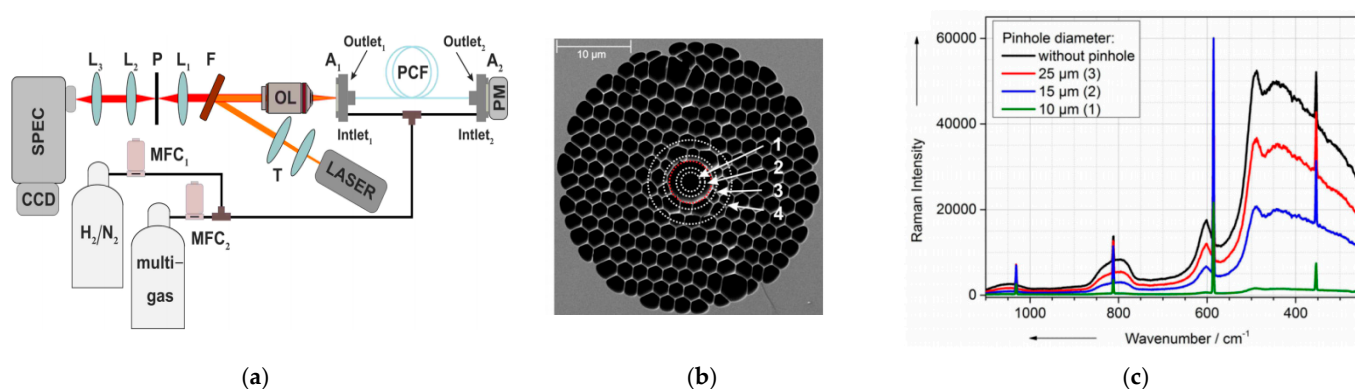


Figure 9. (a) Schematic sketch of the experimental setup for HCPBGF. (b) Electron microscopic picture of the fiber end face. The circular areas marked by '1', '2', '3', and '4' are the collection areas with pinholes sizes of 10, 15, 25, and 50 μm in the focal plane. (c) Raman spectrum of H_2 and the background silica Raman signal of different fibers. Reprinted with permission from [57]. Copyright (2015) American Chemical Society.

Khetani et al. [58] realized the detection of heparin concentration in bovine serum by using HCPBGF, and the Raman signal intensity was more than 90 times stronger than that of direct detection, and strong mode field overlap was achieved by non-selective filling.

However, the hollow hole of the HCPBGF is very small, which limits the speed of the sample in and out, and the sample cannot be switched quickly. Therefore, this kind of fiber is not suitable for high-throughput, online detection applications.

5.2. Hollow Core Anti-Resonant Fiber (HCARF)

The concept of anti-resonance comes from the anti-resonance planar waveguide proposed by Duguay et al. in 1986 [59]. The optical guiding principle of HCARF can be explained by the principle of an anti-resonant reflecting optical waveguide. The light that can be constrained in the fiber is mainly determined by the thickness of the quartz wall in the cladding. When the light is coupled in the core and transmitted to the interface between the core and cladding, the light near the resonant frequency will leak, and other frequencies of light can achieve low loss transmission in the core. That is, the light sandwiched between the specific wavelengths meeting the resonance conditions can be transmitted in the core region, so the region of anti-resonance wavelengths is very wide, which means that the wavelength range transmitted in the core is wide. As the HCARF has a large core and hole spacing, in addition to the advantage of a wide light guide band, it also has low transmission loss, a high damage threshold, single-mode light guide, and other advantages [60].

Due to the photon transmission in the air, the non-linear effect is greatly reduced in HCARF. In addition, HCARF has the characteristics of low transmission loss in the mid-infrared band and a flexible and controllable transmission spectrum [61,62], and is especially suitable for mid-infrared fiber gas lasers. At present, there have been experiments using HCARF for trace detection of gases. In 2018, a high peak power mid-infrared Raman laser output was reported based on a nodeless HCARF with a high-performance near-infrared and mid-infrared broad spectrum light guide [63,64], as shown in Figure 10. Knebl et al. successfully used HCARF for Raman gas sensing and demonstrated its application in environmental science [41,65]. In addition, the research of measuring Raman scattering spectra by HCARF for trace detection is also being developed further [66].

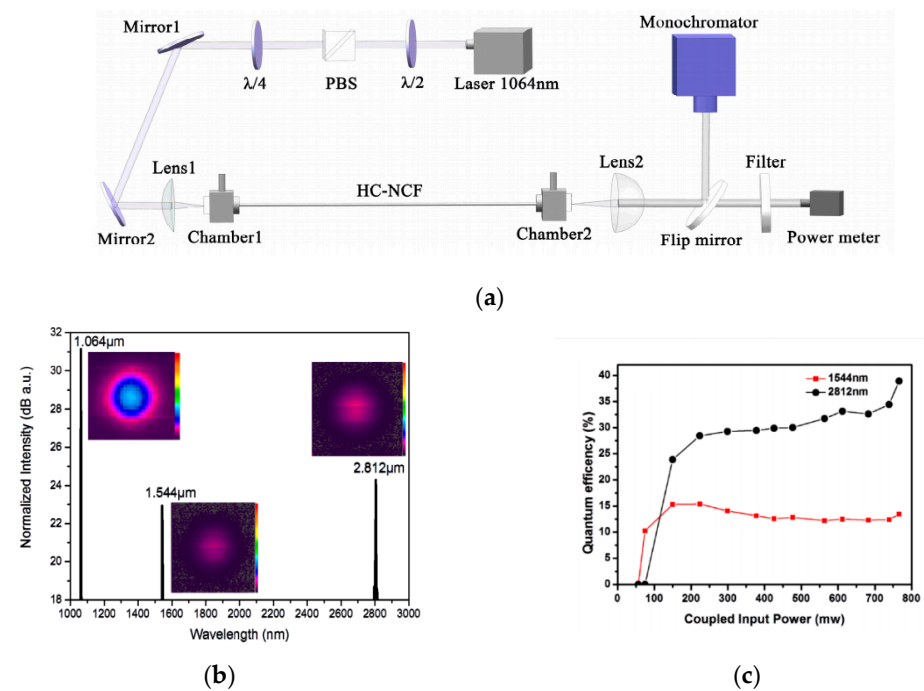


Figure 10. (a) Mid-infrared gas Raman laser device. (b) When the pressure of methane gas is 1.5 MPa and the pumping power is 381 mW, the Raman spectra obtained are inset for the near field mode at the wavelength of 1064, 1544, and 2812 nm. (c) Quantum conversion efficiencies versus the coupled input power at first and second Stokes. Reprinted with permission from [64] © The Optical Society.

6. Capillary-Based Hollow Core Fiber for Raman Sensing

6.1. Metal-Lined Hollow Core Fiber (MLHCF)

For application scenarios that require high time resolution and fast sample switching, HCF with a large core diameter is more suitable. For example, MLHCF has a hollow core aperture of several hundred microns, so there is no need to pressurize when injecting the sample, and its cross-section is shown in Figure 11a. The choice of the plated metal is based on the required transmission conditions. For infrared light waveband transmission, it is preferable to choose a gold-plated film. Silver-plated film and aluminized film are more suitable for visible light waveband transmission and ultraviolet light waveband transmission, respectively [41]. The transmission of light is based on the high reflectance of the metal film. The transmission principle is shown in Figure 11b. Due to multiple reflections of light in the waveguide, the surface roughness or defects of the metal film will cause high loss. The magnitude of the loss is related to the wavelength and the angle of incidence. The shorter the wavelength and the smaller the incident angle, the smaller the loss.

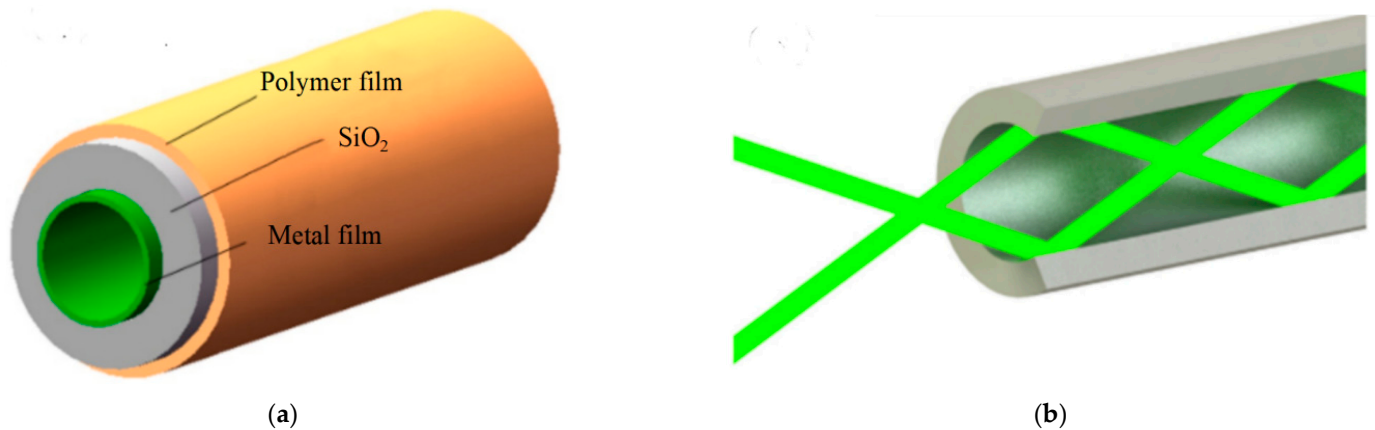


Figure 11. The structure and light guiding principle diagram of MLHCF. (a) Structure diagram. (b) Transmission mechanism of light in MLHCF. Reproduced with permission [10].

Although the MLHCF has a larger transmission loss than the HCPBGF, it can enhance the signal collection efficiency and significantly increase the Raman signal strength, and is used in many detection scenarios. James et al. [67] used the internal silver-plated hollow core fiber (SLHCF) to dynamically monitor trace gases, and realized the real-time detection of various gases during the formation of HD by H₂ and D₂ under the action of a catalyst, with a detection limit of 100 ppm. The device is equipped with metal caps at both ends of the SLHCF to prevent laser light from entering the glass layer of the fiber and reduce the fluorescent background. Pearman et al. [68] used multiple optical fibers to receive the Raman light in the SLHCF, and detected the concentration of N₂, CO₂, and CH₄, and the device is shown in Figure 12a. Compared with the non-silver-plated HCF and the direct detection with a Raman probe, it can be seen from Figure 12b that this method enhanced the Raman signal of non-absorptive gases by 20 times.

In addition, the detection of Raman light in MLHCF needs to consider the effects of fluorescence and background light. The laser optical components and HCF will produce fluorescence, which affects the shot noise of the background spectrum and reduces the signal-to-noise ratio, thereby affecting the detection limit. The most straightforward method can reduce the fluorescence by reducing the number of optical devices, while preventing the spectrometer from receiving the fluorescence from the glass layer. In addition, Okita et al. [69] covered the end face of the HCF, and Mullen et al. [70] coated the end face of the HCF with a layer of silver, which not only prevented the laser from entering the HCF from the end face, but also prevented the glass fluorescence from being received by the spectrometer. In addition, the imperfect optical coupling and transmission loss of

the optical fiber will cause background signals to be generated, causing great problems for trace detection. Rupp et al. [71] studied how to improve the Raman detection limit by reducing the fluorescent background of the MLHCF. The longer the wavelength of the excitation light, the smaller the fluorescence signal of the glass, and the noise can be reduced by adjusting the window structure of the optical device and the Raman cavity in the optical path.

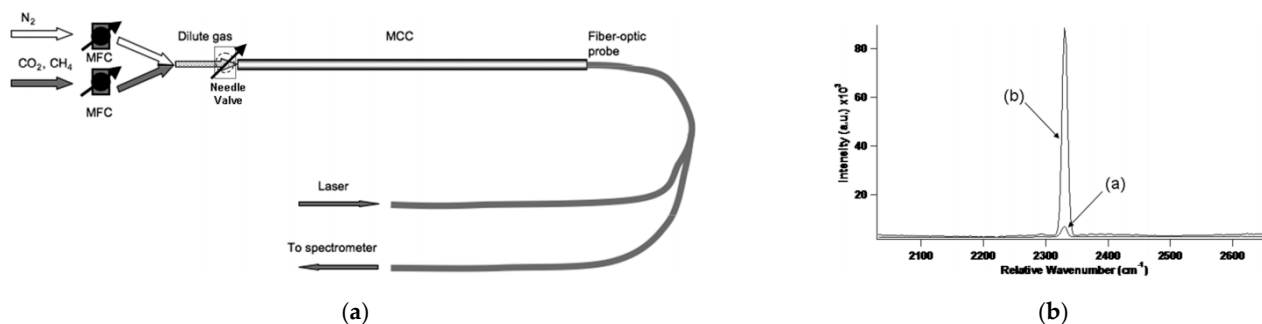


Figure 12. (a) Experimental setup for the collection of MCC Raman scatter. (b) Comparison of experimental results of H₂ in air and MCC. Reprinted with permission from [68] © The Optical Society.

6.1.1. Fabrication Method

The MLHCF used in our studies is the SLHCF produced by Doko Engineering in Japan [72]. The difficulty in manufacturing this kind of optical fiber lies in how to coat the inner wall of the hollow core glass optical fiber with uniform and smooth metallic silver and how to prevent the oxidation of the silver. The company's production principle is to use liquid deposition technology to form metal and dielectric coatings in silicon tubes. Firstly, polyimide film is coated on the outside of the thin-walled silicon tube to enhance the strength of the silicon tube. Secondly, the traditional electroless plating technique is used to deposit a layer of silver in the silicon tube, which includes a mixed silver solution and a retarding fluid. Finally, the dielectric film of silver iodide is formed by the iodine flowing in the tube, that is, the metal and dielectric coatings are formed in the silicon tube. The inner wall of the SLHCF manufactured by this method is smooth, with an average roughness of only 0.04 μm , and low transmission loss and bending loss. Using this method, waveguides with hollow core apertures of 250, 320, 530, and 700 μm and lengths of up to 6 m have been manufactured successfully. This method has simple production process, low cost, and is suitable for mass production.

At the same time, our research group has a set of equipment for MLHCF based on an evaporation method. We chose the VNANO/VZZ-300S high vacuum resistance evaporation coating equipment of Beijing Wiener Vacuum Technology Co., Ltd. to make the coating in house. This method can vapor-deposit the end surface of the part or the outer wall of the glass tube by rotary evaporation. Using this method, after evaporating metal on the outer wall of the glass tube, polyimide or ultraviolet glue is coated on the outside of the metal, and finally hydrofluoric acid is used to corrode the inner glass and the unevenly corroded parts at both ends are cut. With this method, we successfully manufactured gold-plated and aluminized capillaries, but the coating was uneven and the transmission loss was large.

To connect the capillary and the incident fiber (Fiber 1), there are two main methods: free space coupling and inserting coupling [73,74]. In the free space coupling configuration, as shown in Figure 13a, the incident laser is coupled by the convergence of the objective lens. When using this method, the focus position has to be readjusted every time, and the integration of the system is not optimal. In the inserting coupling configuration, as shown in Figure 13b, the incident laser is directly inserted into the capillary, which forms an all-fiber system with high integration. It should be noted that the difference between the inner diameter of the incident fiber and the capillary should be small to minimize the light leakage. Incident laser enters the capillary through Fiber 1 and interacts with the sample

in the capillary to generate the Raman signal. The reflected Raman light is received and detected by Fiber 1 [44].

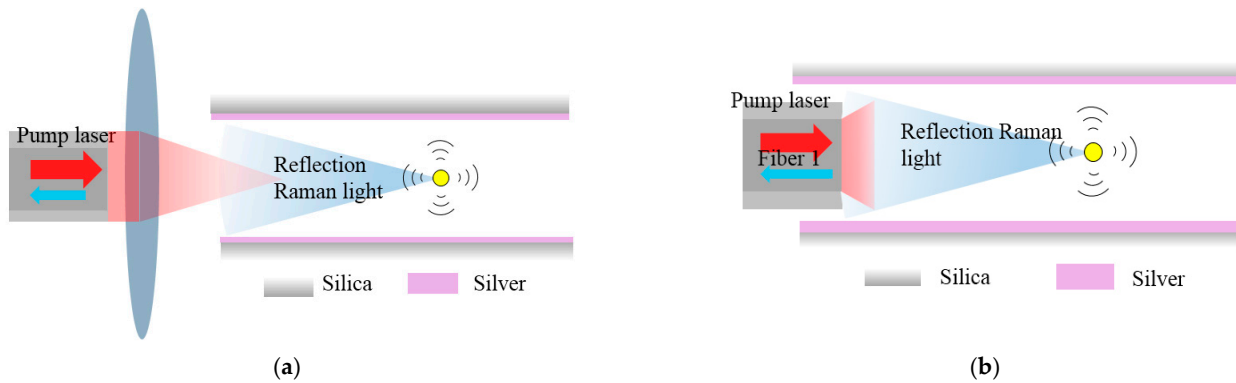


Figure 13. (a) The schematic diagram of free space coupling. (b) The schematic diagram of inserting coupling [10].

6.1.2. Enhancement by Optical Path Configurations

In addition to the enhancement based on different types of optical fibers, further enhancement can be achieved by optical path configurations. As the Raman signal is very weak, MLHCF detection-based enhancement is not sufficient. Therefore, our research group proposed to several optical path configurations, including the addition of a Sagnac loop, capillary with an inserted reflector, and capillary with an inserted FP cavity to enhance the detection of Raman signals in the MLHCF.

- Sagnac Loop

In addition to the enhancement by MLHCF to increase the interaction distance of the light and object for improved Raman light collection efficiency, the Sagnac loop configuration can also collect the reflected and transmitted Raman signals at the same time to further improve the Raman light collection efficiency. The structure of the Sagnac loop is shown in Figure 14a. Two large-core optical fibers are inserted into opposite ends of the SLHCF to form a Raman cavity; the other ends of the optical fibers are tightly glued together to form a Sagnac loop, which is coupled with the Raman probe. The structure diagram of the SLHCF is shown in Figure 14b. The thickness of the silver film is 200 nm, the hollow core aperture is 320 μm, and the outer diameter is 450 μm. The large-core fiber structure is shown in Figure 14c.

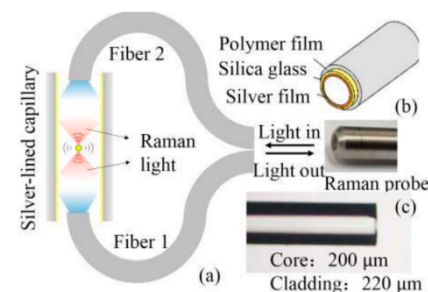


Figure 14. Sagnac ring experimental device diagram. (a) Sagnac loop diagram. (b) Capillary diagram. (c) Large-core diameter fiber after cutting. © (2018) IEEE. Reprinted, with the permission, from [32].

To demonstrate the enhancement by the Sagnac loop structure, a comparison of detecting the Raman signal of isopropanol (ISO) from the Raman probe with and without the Sagnac loop was performed. Firstly, the reflection Raman spectrum from the Raman probe without the Sagnac loop is plotted as the blue line in Figure 15a. Only one fiber was inserted into the capillary and only the reflection Raman spectrum was measured. Next,

equal power was pumped into both fibers in the Sagnac loop structure and the overall Raman spectrum consisting of both transmission and reflection Raman signals is plotted as the yellow line in Figure 15a. The yellow line shows a clear amplification of 3.72 times at 819 cm^{-1} (C-C-O band) while the total excitation optical power doubled in the Sagnac loop configuration [75]. The theoretical analysis suggested an increase of 3.99 times by the Sagnac loop, which matched well with the experimental results. In addition, the device was also demonstrated to detect samples with different concentrations, which proves that the all-fiber Raman cavity has the prospect of realizing online, portable, and fast Raman detection [69,70].

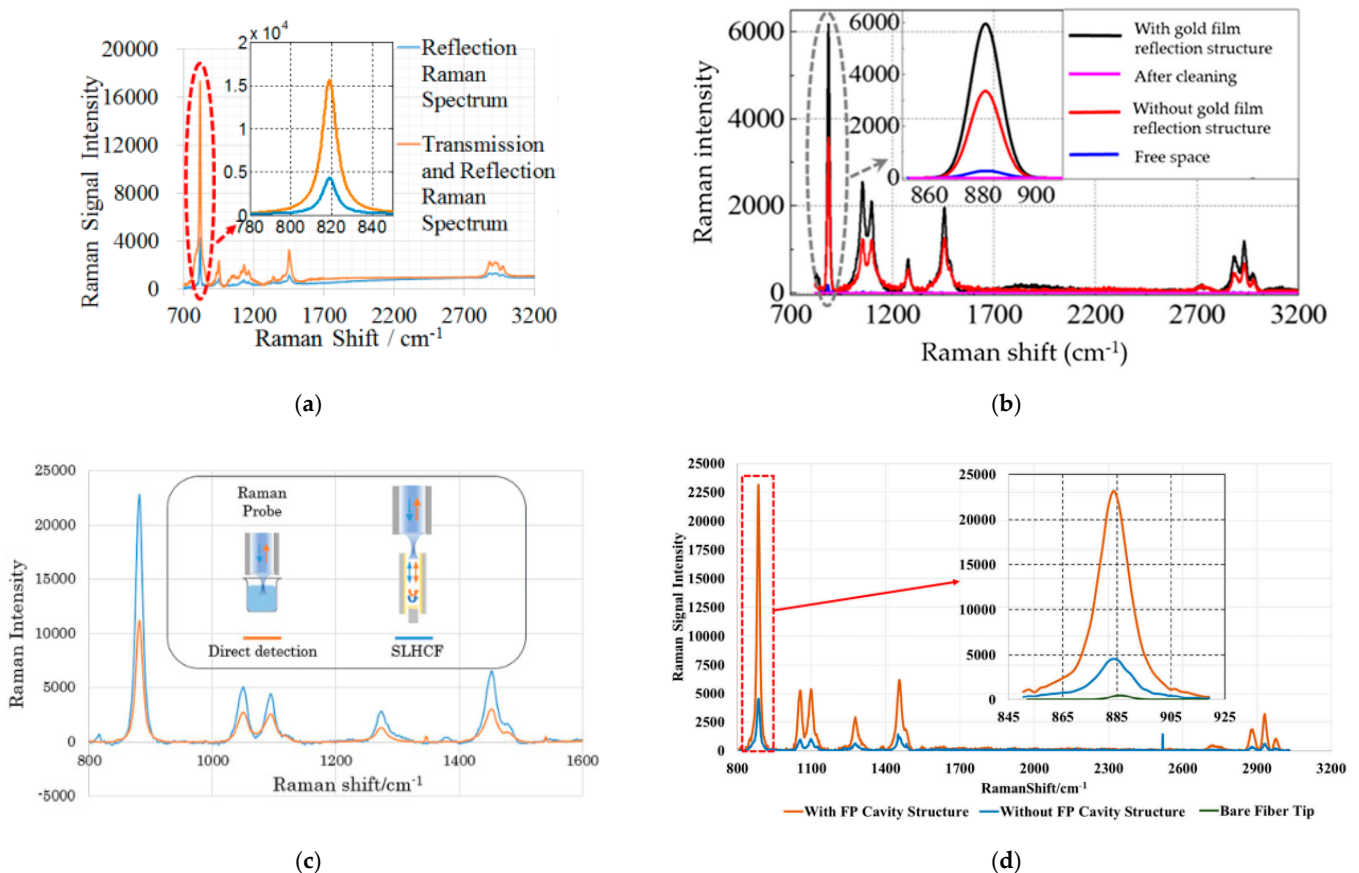


Figure 15. Raman signal enhancement experiment results of different structures. (a) Raman spectrum of ISO in Sagnac loop. © (2018) IEEE. Reprinted, with the permission, from [32]. (b) Raman spectrum of ethanol in capillary with an inserted reflector. Reproduced with permission [10]. (c) Comparison of Raman spectra for ethanol detected by SLHCF and direct detection [27]. (d) Raman spectrum of ethanol in an inserted FP cavity. Reprinted with permission from [46] © The Optical Society.

- Capillary with an inserted reflector

The second optical path configuration is the capillary with an inserted reflector as shown in Figure 16a. The structure used in the experiment is an SLHCF and a gold-plated glass fiber at the end. Two fibers were connected with the capillary by inserting coupling. The experiment used a capillary length of 3 cm and a capillary diameter of 320 μm . The diameter of the gold-plated inserted reflector on the end surface was 275 μm , and the attenuation coefficient was 23 m^{-1} . The experimental parameters and results were used in Formula (13) to calculate the theoretical enhancement ratio of the capillary with an inserted reflector compared with that of the structure without the reflector. The theoretical enhancement factor of 785 nm excitation light was 31.5 times when the cavity length was 3.1 cm. In order to verify the volume enhancement mechanism of the gold film reflection, the experimental parameters remained unchanged. In the case of 785 nm excitation light

power of 36.2 mW and integration time of 2 s, we measured the Raman spectra of ethanol under four different conditions: the SLHCF with gold film reflection structure, the structure after cleaning, the SLHCF without gold film reflection structure, and the free space. The experimental results of the Raman spectrum are shown in Figure 15b.

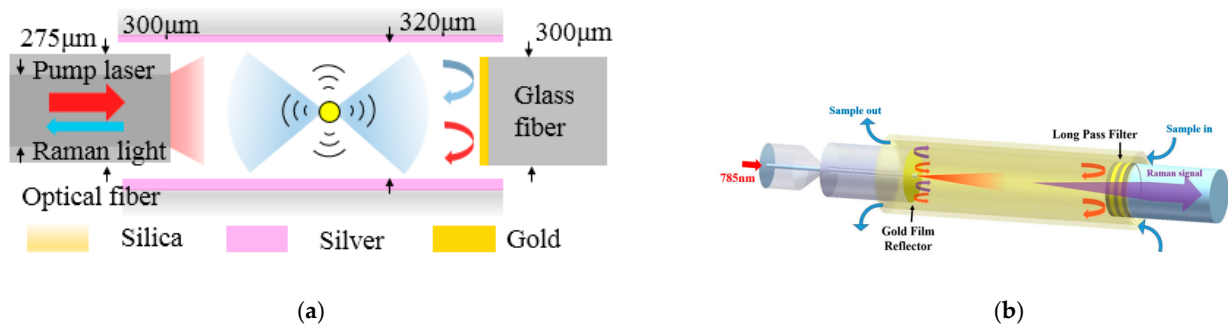


Figure 16. (a) Capillary with an inserted reflector structure diagram [10]. (b) Capillary with an inserted FP cavity detection experimental device structure diagram. Reprinted with permission from [46] © The Optical Society.

First of all, the Raman peak intensity at the Raman frequency shift of 881 cm^{-1} (C-C-O band) based on the SLHCF without the gold film structure was 28 times stronger than that of direct detection in free space. Secondly, the intensity of the Raman peak at 881 cm^{-1} of the gold reflection structure was 1.76 times stronger than that of the SLHCF structure without gold film, so the total volume enhancement factor was 49.3 times. Next, the SLHCF was rinsed with ethanol and deionized water, and subsequently the Raman detection was performed. It can be seen that the sample was completely flushed out of the SLHCF without any residue. In summary, the gold reflection Raman detection device with an inserted reflector has several desirable properties. It can significantly enhance the collected Raman signal compared to the direct detection method. The device can be reused. Furthermore, both the sample entry and exit rates were also fast, which is very suitable for rapid detection application scenarios.

- Capillary with an inserted FP cavity

The capillary with an inserted FP cavity detection is established on the basis of the SLHCF and the end surface reflection structure. The structure is presented in Figure 16b. The FP cavity used a large-core diameter fiber with a gold-plated reflective surface and a 792 nm long-pass coating at both ends. At the output end of the fiber, 46 layers of film were plated on the end face of the large-core fiber with a thickness of 5300 nm, and multilayer materials with different refractive indices separate light with different wavelengths, so as to achieve the effect of separating excitation light and Raman light. The gold-plated reflective surface can reflect the Raman light and the excitation light back into the cavity at the same time, and the long-pass coating only allowed the Raman light whose wavelength is longer relative to the excitation light to pass through, so that the Raman light directly went to the detection unit. The excitation light was reflected back into the cavity, thereby increasing the interaction distance between the light and the substance, and at the same time increasing the collection efficiency of the detection signal.

In order to prove the enhancement effect of SLHCF on signal detection, the comparison of signal strength between SLHCF and direct detection was verified by experiments, and the results are shown in Figure 15c [27].

The experiment detected the Raman signal of ethanol liquid under the conditions of 20 mW excitation light and 10 s integration time. Three different conditions were measured: the SLHCF with FP cavity structure, the SLHCF without FP cavity structure, and bare fiber tip. The experimental results are shown in Figure 15d. The orange lines represent the Raman signal intensity detected in the FP structure, while the blue lines represent no FP cavity structure. The Raman characteristic peak with a bare fiber tip is represented by the

green curve. Compared with the structure without FP cavity, the ethanol Raman signal of the structure with FP cavity was increased by five times. Compared with bare fiber tip, Raman light intensity of the structure with FP cavity was increased by 86 times, which had a good gain effect [46].

6.2. Liquid Core Optical Fiber (LOF)

LOF is a new type of optical transmission element that uses liquid material as the core material and polymer or quartz material as the sheath layer [76]. When the refractive index of the core liquid is higher than the refractive index of the skin tube, the sample can be confined in the waveguide to increase the interaction distance between the light and the substance [77], and increase the optical sensitivity and the efficiency of spectrum collection. LOF also has the advantages of large core diameter, large NA, wide spectrum transmission range, and high light transmission efficiency.

When the cladding material is quartz or glass (the refractive index is about 1.46), the refractive index of the liquid as the core must be greater than 1.46, which severely limits the application of LOF [78]. The new polymer LOF can be designed with a low refractive index cladding. At present, polytetrafluoroethylene (PTFE) material is commonly used as the cladding in LOF. PTFE has excellent chemical stability and corrosion resistance. The refractive index of the PTFE material (Teflon AF2400) produced by DuPont in the United States can be as low as 1.29, and the refractive index of domestic PTFE material is 1.35 [79].

Altcoen et al. designed a tubular LOF entirely made of Teflon AF2400 to measure the Raman spectra of low refractive index liquids [80], and demonstrated LOF filled with water, methanol, ethanol, and acetonitrile. The optical loss was also affected by the defects of the capillary wall and different sections of capillary. When the optical fiber was filled with water, ethanol, and alcohol, the optical loss could be lower than 3 dB/m, 2 dB/m, and 1.9 dB/m, respectively. It was proven that Teflon AF fiber has great advantages in different spectral applications and, even if the loss is high, it can significantly increase the intensity of the Raman spectrum. In 2016, Chiara et al. used 3 m long LOF to measure the linear relationship between ethanol concentration and Raman intensity, and demonstrated that LOF can be used to detect liquid concentration [81], as shown in Figure 17.

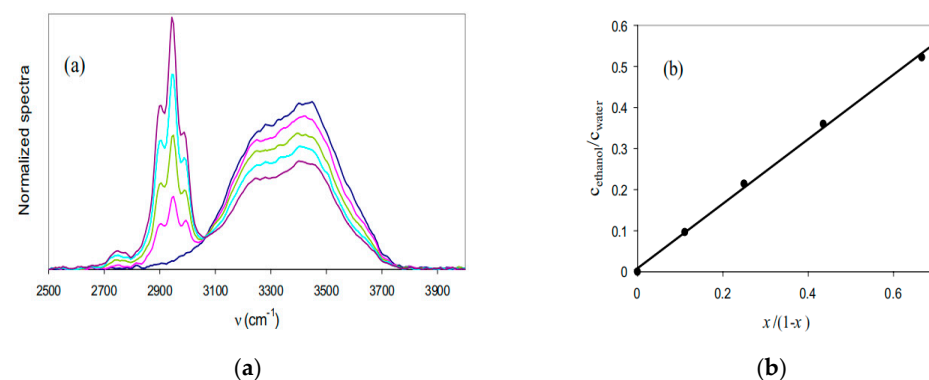


Figure 17. (a) Using LOF to measure the Raman spectra of ethanol at 0, 0.1, 0.2, 0.3, and 0.4 concentrations. The peaks at 2905, 2949, and 2994 cm^{-1} correspond to ethanol. (b) Ethanol/water ratio as a function of the true volume fraction of ethanol x . Errors on the score ratios are less than 1%. Reproduced with permission [81].

Pelletier et al. used LOF made from Teflon AF to measure protein samples and proved that the LOF Raman cavity has a sensitivity enhancement factor of 5009 in aqueous solution under 532 nm excitation light [82]. At present, LOF has been successfully applied to fields including UV curing, UV degradation, UV lithography, forensics, fluorescence detection, UV medical treatment, spectral diagnosis and treatment, etc. [83,84]. Table 2 summarizes the parametric characteristics of the four types of fiber.

Table 2. Comparison of parameters of four optical fibers.

	HCPBGF	HCARF	LOF	MLHCF
Core diameter	Small (5–30 μm)	Medium (20–100 μm) [63]	Large (300–1000 μm)	Large (300–1000 μm)
Bandwidth	Narrow band [85]	Narrow band	All band [86]	All band
Loss	Low (1 dB/km)	Low (50 dB/km)	High (3 dB/m) [80]	Medium (1.2 dB/m) [72]
NA	0.12	0.03	0.54 [87]	0.22 [10]
Detection limit	4.7 ppm [57]	2 ppm [66]	6 ppm [88]	100 ppm [67]
Enhancement factor	10 ⁴ [39]	10 ⁴ [60]	10 ³ –10 ⁴ [89]	10 ³ [90]

7. HCF-based Raman Sensor Applications

7.1. Applications in Gas Detection

In recent years, the application research of gas Raman scattering in various fields has achieved rapid development, and it has broad applications in the fields of sensing, environmental monitoring, gas chemistry research, and medical treatment [91]. As HCF technology becomes more mature, many types of optical fibers become suitable for gas detection, and the performances of optical fibers are getting better. At present, the HCF-based gas Raman light source has achieved multiwavelength Raman output, and the wavelength range also covers the ultraviolet to the mid-infrared. The ultraviolet band has reached 184 nm, and the mid-infrared band has expanded to 4.4 μm. Additionally, distributed gas sensing using stimulated Raman scattering in hydrogen gas-filled HCPCFs has been reported. The distributed Raman gain measurement approach is highly sensitive with a large dynamic range, and both time and spatially resolved. Yang et al. investigated label-free optical fiber distributed Raman hydrogen sensors operating based on stimulated Raman spectroscopy, potentially allowing distributed chemical analysis in gas or liquid phase with high sensitivity and selectivity [92]. Table 3 summarizes the research status of Raman spectroscopy in gas detection in the research community.

Table 3. Examples of gas Raman spectroscopy with HCF.

Year	Research Team	Reference	Pump Wavelength	Fiber Type	Gas	Core Diameter	Enhancement
2008	National Energy Technology Laboratory	[93]	514.5 nm	HCPBGF	N ₂ , O ₂	4.9 μm	Several hundreds
2009		[94]	1302–1637 nm	MLHCF	CO, C ₃ H ₈ , etc.	300 μm	N.A.
2014	Leibniz Institute of Photonic Technology	[57]	670 nm	HCPCF	H ₂ , CH ₄	10, 20, 30 μm	N.A.
2014	University of Bath	[95]	1064 nm	HCPCF	H ₂	53 μm	N.A.
2015	Fusion Science and Technology	[96]	532 nm	MLHCF	H ₂	1 mm	10
2016	Ocean University of China	[97]	532 nm	HCF	O ₂ , N ₂	500 μm	60
2019	The Hong Kong Polytechnic University	[93]	1532 nm	HCPCF	H ₂	10 μm	N.A.
2021	Chongqing University	[67]	532 nm	HCARF	H ₂ , CO, etc.	26 μm	7

7.2. Applications in Liquid Detection

At present, trace detection of liquids is of great significance in the fields of industry, agriculture, and medical treatment, such as monitoring of industrial wastewater discharge, pesticide residues in crops, food additives, body fluid components, pharmaceutical content, etc. It plays a very critical role in maintaining public health and safety and ensuring people's quality of life. However, most of the current liquid detection instruments are large and expensive, and are not suitable for fast and convenient online detection. The volume enhancement effect of HCF can realize efficient and rapid detection of Raman spectroscopy of substances. LOF, MLHCF, and HCPCF have all made progress in liquid Raman spectroscopy detection, as summarized in Table 4.

Table 4. Examples of liquid Raman spectroscopy with HCF.

Year	Research Team	Reference	Pump Wavelength	Fiber Type	Liquid	Core Diameter	Enhancement
1997	Northwestern University	[80]	632.8 nm	LOF	Water, methanol, ethanol, acetonitrile	250 μm	N.A.
2001	Northwestern University	[82]	532 nm	LOF	Water protein	50 μm	500
2011	University of Ottawa	[58]	785 nm	HCPCF	Heparin	10.6 μm	90
2017	Leibniz Institute of Photonic Technology	[53]	532, 676, 752 nm	HCPCF	Ethanol	20 μm	10
2020	Nanjing University	[10]	785 nm	MLHCF	Ethanol	125 μm	4.83

7.3. Application in Medicine

Biological liquids provide a wealth of information about human health. The HCF-based Raman detection technology for detection of biological liquids can achieve applications in immunity and biochemistry. In 2017, Qi et al. reported a method using LOF to measure the chemical concentration in clinical serum and urine samples based on Raman spectra and absorption spectra in the near-infrared region [98]. The experimental setup is shown in Figure 18. The LOF used therein has a length of 30 cm and an inner and outer diameter of 600 μm and 800 μm , so the total volume is less than 0.1 mL. The laser power at the entrance of the LOF is about 160 mW. This method can automatically analyze the samples and predict the concentration of most samples within the accuracy range of the clinical reference analyzer, which has a huge potential in biochemical medicine. In 2019, Xiao et al. designed a device for detecting bisphenol A in blood and environmental samples using the superior physicochemical properties of the HCARF and the two-dimensional material black phosphorus. The detection limit increased by more than two orders of magnitude compared to traditional devices [99]. In addition, Azkune et al. used a 66 μm LOF to achieve the quantitative detection of low-concentration glucose, with a detection limit as low as 0.0186 mol/L, proving that this method is suitable for detecting clinically relevant glucose concentrations and, in the treatment of SGLT2 inhibitors, it has shown great potential for urine glucose monitoring [100].

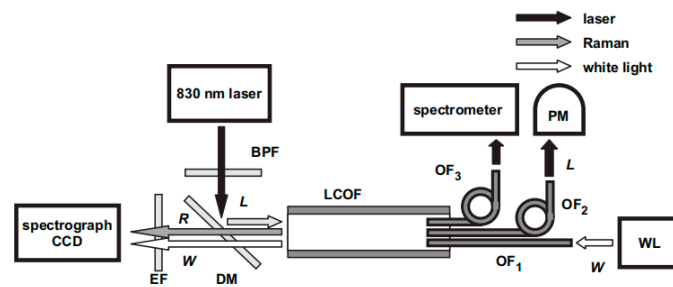


Figure 18. The experimental device for detecting Raman spectra and absorption spectra using LOF. Reprinted with permission from [98] © The Optical Society.

8. Prospect and Conclusions

This article summarizes the research of all-fiber online Raman sensors with hollow core microstructured optical fibers. In comparison with other Raman signal enhancement techniques, FERS has demonstrated attractive capabilities and great potential to achieve rapid online Raman detection. Four different types of HCFs are reviewed in detail, showing their configurations, theoretical analyses, fabrication, experimental results, and application demonstrations for fast online Raman spectroscopy with significant signal enhancement. The HCF detection method is used to make up for the weak Raman signal and the signal enhancement is up to 10,000 times higher than that of direct detection. In addition, the system can be used many times, is easy to clean and does not have residual crosstalk, and the detection speed is as fast as a few seconds, so it is suitable for online real-time material detection, such as for safety inspection, food detection, water quality detection, etc.

In the future, the all-fiber online Raman sensor with hollow core microstructured optical fiber system has a lot of room for improvement in signal enhancement and usage scenarios. In order to enhance the resolution of the Raman signal and reduce the background noise during detection, the hollow fiber detection technology can be combined with other detection enhancement methods such as SERS, related Raman methods such as stimulated Raman, and new fiber types. In terms of application scenarios, this technology can be combined with microfluidic technology and installed in the detection part after sample pretreatment; it can also be combined with magnetic beads and external magnetic force to achieve magnetic enrichment and purification. Combined with artificial intelligence and machine learning to analyze spectral data, a complete set of sample detection procedures can be realized.

Furthermore, recent innovations and continuous development of the laser technologies with new wavelengths and time resolutions open up new opportunities for Raman sensors. For example, UV Raman can effectively reduce the fluorescence interference in the Raman signal. Nanosecond and picosecond lasers improve the time resolution of Raman spectroscopy and further expand the application range of Raman spectroscopy. In addition to the qualitative and quantitative analysis of the substances mentioned in this article, Raman spectroscopy technology has certain advantages in the fields of medical biology, molecular microdynamics, archaeology, etc. Moving forward, with the further innovation and development of experimental and theoretical methods, Raman spectroscopy technology will become a powerful tool for biological and chemical technology and applications.

Author Contributions: Conceptualization: D.J.J.H., G.W. and X.Y. writing—original draft preparation, H.D. and X.Y.; writing—review and editing: H.D., D.J.J.H., G.W., X.L. and Y.Z. All authors have read and agreed to the published version of the manuscript.

Funding: This work was sponsored by National Natural Science Foundation of China (nos. 61875083, 61535005), and Social Development Project of Jiangsu Province (BE2019761).

Institutional Review Board Statement: Not applicable.

Informed Consent Statement: Not applicable.

Data Availability Statement: Not applicable.

Conflicts of Interest: The authors declare no conflict of interest.

References

1. Lee, K.S.; Landry, Z.; Pereira, F.C.; Wagner, M.; Berry, D.; Huang, W.E.; Taylor, G.T.; Kneipp, J.; Popp, J.; Zhang, M.; et al. Raman microspectroscopy for microbiology. *Nat. Rev. Methods Primers* **2021**, *1*, 80. [[CrossRef](#)]
2. Ho, C.-S.; Jean, N.; Hogan, C.A.; Blackmon, L.; Jeffrey, S.S.; Holodniy, M.; Banaei, N.; Saleh, A.A.E.; Ermon, S.; Dionne, J. Rapid identification of pathogenic bacteria using Raman spectroscopy and deep learning. *Nat. Commun.* **2019**, *10*, 4927. [[CrossRef](#)]
3. Kassa-Baghdouche, L.; Cassan, E. Mid-infrared refractive index sensing using optimized slotted photonic crystal waveguides. *Photon. Nanostruct. Fundam. Appl.* **2018**, *28*, 32–36. [[CrossRef](#)]
4. Kassa-Baghdouche, L.; Cassan, E. Sensitivity analysis of ring-shaped slotted photonic crystal waveguides for mid-infrared refractive index sensing. *Opt. Quantum Electron.* **2019**, *51*, 328. [[CrossRef](#)]
5. Wu, L.; Ouyang, Z.H.; Cao, S.C. Research development and application of Raman scattering technology. *Chin. J. Light Scatt.* **2005**, *17*, 180–186.
6. Schwab, S.D.; McCreery, R.L. Remote, long-pathlength cell for high-sensitivity Raman spectroscopy. *Appl. Spectrosc.* **1987**, *41*, 126–130. [[CrossRef](#)]
7. Raman, C.V.; Krishnan, K.S. The optical analogue of the Compton effect. *Nature* **1928**, *121*, 711. [[CrossRef](#)]
8. Kudelski, A. Analytical applications of Raman spectroscopy. *Talanta* **2008**, *76*, 1–8. [[CrossRef](#)]
9. Rostron, P.; Gerber, D. Raman spectroscopy, a review. *Int. J. Eng. Tech. Res.* **2016**, *6*, 50–64.
10. Chu, Q. Enhanced Raman Detection Based on the Metal-lined Hollow-Core Fiber. Master's Thesis, Nanjing University, Nanjing, China, 2019.
11. Harvey, B.; Coherent, A. Anti-Stokes Raman spectroscopy. *Anal. Chem.* **1978**, *50*, 905A–912A. [[CrossRef](#)]
12. Hercher, M.; Mueller, W.; Klainer, S.; Adamowicz, R.F.; Schwartz, S.E. An efficient intracavity laser Raman spectrometer. *Appl. Spectrosc.* **1978**, *32*, 298–302. [[CrossRef](#)]
13. Fleischmann, M.P.; Hendra, P.J.; McQuillan, A.J. Raman spectra of pyridine adsorbed at a silver electrode. *Chem. Phys. Lett.* **1974**, *26*, 163–166. [[CrossRef](#)]
14. Johannessen, C.; White, P.C.; Abdali, S. Resonance Raman optical activity and surface enhanced resonance Raman optical activity analysis of cytochrome C. *J. Phys. Chem. A* **2007**, *111*, 7771–7776. [[CrossRef](#)]
15. Spiro, T.G.; Streckas, T.C. Resonance Raman spectra of heme proteins. Effects of oxidation and spin state. *J. Am. Chem. Soc.* **1974**, *96*, 338–345. [[CrossRef](#)] [[PubMed](#)]
16. Maker, P.D.; Terhune, R.W. Study of optical effects due to an induced polarization third order in the electric field strength. *Phys. Rev.* **1965**, *137*, 801–818. [[CrossRef](#)]
17. Cheng, J.X.; Xie, X.S. Coherent anti-Stokes Raman scattering microscopy: Instrumentation, theory, and applications. *J. Phys. Chem. B* **2004**, *108*, 827–840. [[CrossRef](#)]
18. Roy, S.; Gord, J.R.; Patnaik, A.K. Recent advances in coherent anti-Stokes Raman scattering spectroscopy: Fundamental developments and applications in reacting flows. *Prog. Energy Combust. Sci.* **2010**, *36*, 280–306. [[CrossRef](#)]
19. King, D.A.; Pittaro, R.J. Simple diode pumping of a power-buildup cavity. *Opt. Lett.* **1998**, *23*, 774. [[CrossRef](#)] [[PubMed](#)]
20. Taylor, D.J.; Glugla, M.; Penzhorn, R.D. Enhanced Raman sensitivity using an actively stabilized external resonator. *Rev. Sci. Instrum.* **2001**, *72*, 1970–1976. [[CrossRef](#)]
21. Campion, A.; Kambhampati, P. Surface-enhanced Raman scattering. *Chem. Soc. Rev.* **1998**, *27*, 241–250. [[CrossRef](#)]
22. Stockle, R.M.; Suh, Y.D.; Deckert, V.; Zenobi, R. Nanoscale chemical analysis by tip-enhanced Raman spectroscopy. *Chem. Phys. Lett.* **2000**, *318*, 131–136. [[CrossRef](#)]
23. Pettinger, B.; Picardi, G.; Schuster, R.; Ertl, G. Surface-enhanced and STM tip-enhanced Raman spectroscopy of CN⁻ ions at gold surfaces. *J. Electroanal. Chem.* **2003**, *554–555*, 293–299. [[CrossRef](#)]
24. Neacsu, C.C.; Dreyer, J.; Behr, N.; Raschke, M.B. Scanning-probe Raman spectroscopy with single-molecule sensitivity. *Phys. Rev. B* **2006**, *73*, 193406. [[CrossRef](#)]
25. Moskovits, M. Surface-enhanced Raman spectroscopy: A brief retrospective. *J. Raman Spectrosc.* **2010**, *36*, 485–496. [[CrossRef](#)]
26. Pettinger, B.; Ren, B.; Picardi, G.; Schuster, R.; Ertl, G. Nanoscale probing of adsorbed species by tip-enhanced Raman spectroscopy. *Phys. Rev. Lett.* **2004**, *92*, 096101. [[CrossRef](#)]
27. Cai, H.; Yu, X.T.; Chu, Q.; Jin, Z.Q.; Lin, B.; Wang, G.H. Hollow-core fiber-based Raman probe extension kit for in situ and sensitive ultramicro-analysis. *Chin. Opt. Lett.* **2019**, *17*, 5–9. [[CrossRef](#)]
28. Zhang, N.Q.; Qin, T.L.; Wang, Z.F.; Liu, W.B.; Cao, J.Q.; Chen, Z.L. Low-loss coupling between tapered fibers and anti-resonant hollow-core photonic crystal fibers. *Laser Optoelectron. Prog.* **2017**, *54*, 100608. [[CrossRef](#)]
29. Shephard, J.D.; Macpherson, W.N.; Maier, R.R.J.; Jones, J.D.C.; Knight, J.C. Single-mode mid-IR guidance in a hollow-core photonic crystal fiber. *Opt. Express* **2005**, *13*, 7139–7144. [[CrossRef](#)]
30. Zhang, W.; Lou, S.; Wang, X.; Yan, S.; Xing, Z. A broadband single mode single polarization metal wires-embedded hollow core anti-resonant fiber for polarization filter. *Opt. Fiber Technol.* **2019**, *53*, 102011. [[CrossRef](#)]

31. Salter, R.; Chu, J.; Hippler, M. Cavity-enhanced Raman spectroscopy with optical feedback cw diode lasers for gas phase analysis and spectroscopy. *Analyst* **2012**, *137*, 4669–4676. [[CrossRef](#)]
32. Jin, Z.; Chu, Q.; Xu, W.; Cai, H.; Ji, W.; Wang, G.; Lin, B.; Zhang, X. All-fiber Raman biosensor by combining reflection and transmission mode. *IEEE Photon. Technol. Lett.* **2018**, *30*, 387–390. [[CrossRef](#)]
33. Zhang, Z.M.; Chen, S.; Liang, Y.Z.; Liu, Z.X.; Zhang, Q.M.; Ding, L.X.; Ye, F.; Zhou, H. An intelligent background-correction algorithm for highly fluorescent samples in Raman spectroscopy. *J. Raman Spectrosc.* **2010**, *41*, 659–669. [[CrossRef](#)]
34. Gambling, W.A.; Payne, D.N.; Matsumura, H. Gigahertz bandwidths in multimode, liquid-core, optical fibre waveguide. *Opt. Commun.* **1972**, *6*, 317–322. [[CrossRef](#)]
35. Stone, J. Optical transmission in liquid-core quartz fibers. *Appl. Phys. Lett.* **1972**, *20*, 239–241. [[CrossRef](#)]
36. Ogilvie, G.J.; Esdaile, R.J.; Kidd, G.P. Transmission loss of tetrachloroethylene-filled liquid-core-fibre light guide. *Electron. Lett.* **1972**, *8*, 533–534. [[CrossRef](#)]
37. Ippen, E.P. Low-power quasi-cw Raman oscillator. *Appl. Phys. Lett.* **1970**, *16*, 303–305. [[CrossRef](#)]
38. Walrafen, G.E.; Stone, J. Intensification of spontaneous Raman spectra by use of liquid core optical fibers. *Appl. Spectrosc.* **1972**, *26*, 585–589. [[CrossRef](#)]
39. Fuwa, K.; Lei, W.; Fujiwara, K. Colorimetry with a total-reflection long capillary cell. *Anal. Chem.* **1984**, *56*, 1640–1644. [[CrossRef](#)]
40. Fujiwara, K.; Simeonsson, J.B.; Smith, B.W.; Winefordner, J.D. Waveguide capillary flow cell for fluorometry. *Anal. Chem.* **1988**, *60*, 1065–1068. [[CrossRef](#)]
41. Knebl, A.; Yan, D.; Popp, J.; Frosch, T. Fiber enhanced Raman gas spectroscopy. *TrAC Trends Anal. Chem.* **2017**, *103*, 230–238. [[CrossRef](#)]
42. Frosch, T.; Di, Y.; Popp, J. Ultrasensitive fiber enhanced UV resonance Raman sensing of drugs. *Anal. Chem.* **2013**, *85*, 6264–6271. [[CrossRef](#)] [[PubMed](#)]
43. Chu, Q.; Jin, Z.; Yu, X.; Li, C.; Zhang, W.; Ji, W.; Lin, B.; Shum, P.P.; Zhang, X.; Wang, G. Volumetric enhancement of Raman scattering for fast detection based on a silver-lined hollow-core fiber. *Opt. Express* **2019**, *27*, 10370–10382. [[CrossRef](#)] [[PubMed](#)]
44. Jin, Z.Q.; Chu, Q.; Fan, D.Y.; Xu, W.H.; Cai, H.; Wang, G.H.; Xu, F.; Lin, B.; Zhang, X. All fiber on-line Raman detection system with silver-coated hollow fiber. In Proceedings of the 2017 16th International Conference on Optical Communications & Networks (ICOON), Wuzhen, China, 7–10 August 2017; IEEE: Manhattan, NY, USA, 2017.
45. Chu, Q.; Wang, G.H.; Jin, Z.Q.; Tan, J.; Cai, H.; Lin, B.; Zhang, X. All-fiber, portable, online Raman biosensor with enhancement of signal excitation and collection efficiency. In Proceedings of the 2018 Conference On Lasers and Electro-Optics (CLEO), San Jose, CA, USA, 13–18 May 2018; IEEE: Manhattan, NY, USA, 2018.
46. Yu, X.T.; Li, C.X.; Hu, D.J.J.; Milenko, K.; Wang, G.H.; Shum, P.; Xu, F.; Lu, Y.Q.; Zhang, X.P. All-fiber online Raman sensor with enhancement via a fabry-perot cavity. *Opt. Lett.* **2020**, *45*, 5760–5763. [[CrossRef](#)]
47. Russell, P. Photonic crystal fibers. *Science* **2003**, *299*, 358–362. [[CrossRef](#)]
48. Benabid, F. Hollow-core photonic bandgap fibre: New light guidance for new science and technology. *Philos. Trans. Math. Phys. Eng. Sci.* **2006**, *364*, 3439–3462. [[CrossRef](#)]
49. Cheng, T.L.; Li, S.G.; Zhou, G.Y.; Hou, L.T. Relation between power fraction in the core of hollow-core photonic crystal fibers and their bandgap property. *Chin. J. Lasers* **2007**, *34*, 249.
50. Roberts, P.J.; Couny, F.; Sabert, H.; Mangan, B.J.; Russell, P.S.J. Ultimate low loss of hollow-core photonic crystal fibres. *Opt. Express* **2005**, *13*, 236–244. [[CrossRef](#)]
51. Guo, X.R.; Yang, D.X. Propagating light with the full cladding of hollow-core photonic crystal fiber. *J. Appl. Opt.* **2011**, *32*, 744–748.
52. Yuan, J.H.; Hou, L.T.; Wei, D.B.; Wang, H.Y.; Zhou, G.Y. Experimental investigation and the application of hollow-core photonic crystal fiber in visible range. *J. Optoelectron. Laser* **2008**, *09*, 1150–1153.
53. Yan, D.; Popp, J.; Pletz, M.W.; Frosch, T. Highly sensitive broadband Raman sensing of antibiotics in step-index hollow-core photonic crystal fibers. *ACS Photonics* **2017**, *4*, 138–145. [[CrossRef](#)]
54. He, D.D.; Liu, M.; Jian, D.; Li, D.; Liao, Z.Y. Study on loss in hollow-core photonic bandgap fibers. *Laser Technol.* **2013**, *37*, 243–246.
55. Saitoh, K.; Koshiba, M. Confinement losses in air-guiding photonic bandgap fibers. *IEEE Photonics Technol. Lett.* **2003**, *15*, 236–238. [[CrossRef](#)]
56. Kim, H.K.; Digonnet, M.; Kino, G.S.; Shin, J.; Fan, S. Simulations of the effect of the core ring on surface and air-core modes in photonic bandgap fibers. *Opt. Express* **2004**, *12*, 3436–3442. [[CrossRef](#)]
57. Hanf, S.; Bogozi, T.; Keiner, R.; Frosch, T.; Popp, J. Fast and highly sensitive fiber-enhanced raman spectroscopic monitoring of molecular H₂ and CH₄ for point-of-care diagnosis of malabsorption disorders in exhaled human breath. *Anal. Chem.* **2015**, *87*, 982–988. [[CrossRef](#)]
58. Khetani, A.; Tiwari, V.S.; Harb, A.; Anis, H. Monitoring of heparin concentration in serum by Raman spectroscopy within hollow core photonic crystal fiber. *Sch. Inf. Technol. Eng. (SITE)* **2011**, *19*, 15244–15254. [[CrossRef](#)]
59. Duguay, M.A.; Kokubun, Y.; Koch, T.L.; Pfeiffer, L. Antiresonant reflecting optical waveguides in SiO₂-Si multilayer structures. *Appl. Phys. Lett.* **1986**, *49*, 13–15. [[CrossRef](#)]
60. Cao, L. Mid-Infrared Gas Raman Laser Source Based on Hollow-Core Anti-Resonant Fiber. Master's Thesis, Beijing University of Technology, Chaoyang, China, 2018.
61. Fei, Y.; Wadsworth, W.J.; Knight, J.C. Low loss (34 dB/km) silica hollow core fiber for the 3 μm spectral region. In Proceedings of the Specialty Optical Fibers, Colorado Springs, CO, USA, 17–21 June 2012.

62. Yu, F.; Knight, J.C. Spectral attenuation limits of silica hollow core negative curvature fiber. *Opt. Express* **2013**, *21*, 21466–21471. [[CrossRef](#)]
63. Gao, S.F.; Wang, Y.Y.; Wang, P. Research progress on hollow-core anti-resonant fiber and gas raman laser technology. *Chin. J. Lasers* **2019**, *46*, 183–200.
64. Ling, C.; Gao, S.F.; Peng, Z.G.; Wang, X.C.; Pu, W. High peak power 2.8 μm Raman laser in a methane-filled negative-curvature fiber. *Opt. Express* **2018**, *26*, 5609–5615.
65. Knebl, A.; Domes, R.; Wolf, S.; Domes, C.; Popp, J.; Frosch, T. Fiber-enhanced Raman gas spectroscopy for the study of microbial methanogenesis. *Anal. Chem.* **2020**, *92*, 12564–12571. [[CrossRef](#)]
66. Wang, J.X.; Chen, W.G.; Wan, F.; Wang, P.; Zhang, R. Fiber-enhanced Raman spectroscopic monitoring of fault characteristic gases dissolved in transformer oil by hollow-core photonic crystal fiber. In Proceedings of the 2018 IEEE International Conference on High Voltage Engineering and Application (ICHVE), Athens, Greece, 10–13 September 2018.
67. James, T.M.; Rupp, S.; Telle, H.H. Trace gas and dynamic process monitoring by Raman spectroscopy in metal-coated hollow glass fibres. *Anal. Methods* **2015**, *7*, 2568–2576. [[CrossRef](#)]
68. Pearman, W.F.; Carter, J.C.; Angel, S.M.; Chan, W.J. Quantitative measurements of CO_2 and CH_4 using a multipass Raman capillary cell. *Appl. Opt.* **2008**, *47*, 4627–4632. [[CrossRef](#)] [[PubMed](#)]
69. Okita, Y.; Gannot, I.; Katagiri, T.; Matsuura, Y. A Raman cell based on hollow optical fibers for breath analysis. In Proceedings of the Optical Fibers and Sensors for Medical Diagnostics and Treatment Applications X, San Francisco, CA, USA, 23–28 January 2010; Volume 7559, pp. 42–46.
70. Mullen, J.C.; Buric, M.P.; Chorpeneing, B.T.; Woodruff, S.D. Azimuthal polarization for Raman enhancement in capillary waveguides. *Opt. Eng.* **2013**, *52*, 117103. [[CrossRef](#)]
71. Simone, R.; Andreas, O.; Hendrik, S.M.; Timothy, J.; Helmut, T. Improving the detection limit in a capillary raman system for in situ gas analysis by means of fluorescence reduction. *Sensors* **2015**, *15*, 23110–23125.
72. Matsuura, Y.; Abel, T.; Harrington, J.A. Optical properties of small-bore hollow glass waveguides. *Appl. Opt.* **1995**, *34*, 6842–6847. [[CrossRef](#)] [[PubMed](#)]
73. Fan, D.; Jin, Z.; Wang, G.; Xu, F.; Lu, Y.; Hu, D.J.J.; Wei, L.; Shum, P.; Zhang, X. Extremely high-efficiency coupling method for hollow-core photonic crystal fiber. *IEEE Photonics J.* **2017**, *9*, 1–8. [[CrossRef](#)]
74. Fan, D.Y. Research on On-Line Raman Detecting System Based on Hollow-Core Fiber. Master's Thesis, Nanjing University, Nanjing, China, 2017.
75. Liu, Z.Q.; Wang, Y.J.; Lu, X.B.; Kan, M.X. Determination of isopropanol content by laser Raman spectroscopic internal standard method. In Proceedings of the National Conference on Chemistry and Spectroscopic Analysis, Chengdu, China, 29 July–2 August 2011.
76. Xu, Y.; Chen, X.; Zhu, Y. High sensitive temperature sensor using a liquid-core optical fiber with small refractive index difference between core and cladding materials. *Sensors* **2008**, *8*, 1872–1878. [[CrossRef](#)]
77. Huo, L.; Lin, C.; Suen, Y.K.; Kong, S.K. Raman signal enhancement in a liquid-core optical fiber based on hollow-core photonic crystal fiber. In Proceedings of the 2007 Asia Optical Fiber Communication and Optoelectronics Conference, Shanghai, China, 17–19 October 2007; pp. 233–235.
78. Wang, W.; Feng, M.Z. Characteristics of low-refractive-index liquid-core optical fibers. *J. Translucation Technol.* **1996**, *01*, 15–18.
79. Fan, Y.; Wu, R.M.; Ai, S.R.; Liu, M.H.; Yang, H.F.; Zheng, J.H. Identification study of edible oil species with laser induced fluorescence technology based on liquid core optical fiber. *Spectrosc. Spectr. Anal.* **2016**, *36*, 3202–3206.
80. Altkorn, R.; Koev, I.; Duyne, R.; Litorja, M. Low-loss liquid-core optical fiber for low-refractive-index liquids: Fabrication, characterization, and application in Raman spectroscopy. *Appl. Opt.* **1997**, *36*, 8992–8998. [[CrossRef](#)]
81. Meneghini, C.; Caron, S.; Proulx, A.; Emond, F.; Paradis, P.; Pare, C.; Fougères, A. Ethanol concentration measurement by Raman spectroscopy in liquid-core microstructured optical fiber. In *Third European Workshop on Optical Fibre Sensors*; Cutolo, A., Culshaw, B., LopezHiguera, J.M., Eds.; SPIE: Bellingham, WA, USA, 2007; Volume 6619.
82. Pelletier, M.J.; Altkorn, R. Raman sensitivity enhancement for aqueous protein samples using a liquid-core optical-fiber cell. *Anal. Chem.* **2001**, *73*, 1393–1397. [[CrossRef](#)] [[PubMed](#)]
83. Ramza, H.; Arsad, N.; Abdurrahman, F.; Supian, L.S.; Ab-Rahman, M.S. Optical fiber pressure sensor using extrinsic Fabry-Perot interferometry (EFPI): A theoretical study. *J. Optoelectron. Adv. Mater.* **2015**, *17*, 545–551.
84. Bethoux, O.; Godoy, E.; Roche, I.; Naccari, B.; Taleb, M.A.; Koteiche, M.; Nassif, Y. A new state-observer of the inner PEM fuel cell pressures for enhanced system monitoring. *Eur. Phys. J. Appl. Phys.* **2014**, *66*, 30901. [[CrossRef](#)]
85. AmezcuaCorrea, R.; Leonsaval, S.; Birks, T.; Knight, J.C. Control of surface modes in low loss hollow-core photonic bandgap fibers. *Opt. Express* **2008**, *16*, 1142–1149. [[CrossRef](#)]
86. Shen, L.B.; Zhang, X.N. A study on novel liquid-core fiber and its properties. *J. Jinling Inst. Technol.* **2018**, *34*, 25–28.
87. Ishiharada M, N.K.; Tanuma, I.; Matsumuro, Y.; Honda, T. Properties of flexible light guide made of liquid core and polymer clad. *Plast. Opt. Fibres Appl.* **1993**, 49–53.
88. Marquardt, B.J.; Turney, K.P.; Burgess, L.W. Raman waveguide detector for low analyte concentrations in liquid samples. In Proceedings of the SPIE—The International Society for Optical Engineering, Boston, MA, USA, 19–22 September 1999; Volume 3860, pp. 239–249.

89. Gao, S.Q.; Li, Z.W.; Zhang, W.; Li, J.N. Liquid core optical fiber preresonance and resonance raman spectroscopy and its application. *Chin. J. Anal. Chem.* **1997**, *25*, 4.
90. Jin, Z.Q. On-Line Raman Liquid Detecting Methods Based on Hollow-Core Fiber. Master's Thesis, Nanjing University, Nanjing, China, 2018.
91. Pearman, W.F.; Carter, J.C.; Angel, S.M.; Chan, W.J. Multipass capillary cell for enhanced raman measurements of gases. *Appl. Spectrosc.* **2015**, *62*, 285–289. [[CrossRef](#)]
92. Yang, F.; Zhao, Y.; Qi, Y.; Tan, Y.Z.; Ho, H.L.; Jin, W. Towards label-free distributed fiber hydrogen sensor with stimulated Raman spectroscopy. *Opt. Express* **2019**, *27*, 12869–12882. [[CrossRef](#)]
93. Buric, M.P.; Chen, K.P.; Falk, J.; Woodruff, S.D. Enhanced spontaneous Raman scattering and gas composition analysis using a photonic crystal fiber. *Appl. Opt.* **2008**, *47*, 4255–4261. [[CrossRef](#)]
94. Buric, M.P.; Chen, K.; Falk, J.; Velez, R.; Woodruff, S. Raman sensing of fuel gases using a reflective coating capillary optical fiber. *Proc. SPIE* **2009**, *7316*, 433–443.
95. Wang, Z.; Yu, F.; Wadsworth, W.J.; Knight, J.C. Efficient 1.9 μm emission in H₂-filled hollow core fiber by pure stimulated vibrational Raman scattering. *Laser Phys. Lett.* **2014**, *11*, 105807. [[CrossRef](#)]
96. Rupp, S.; James, T.M.; Telle, H.H.; Schloesser, M.; Bornschein, B. Enhanced sensitivity of raman spectroscopy for tritium gas analysis using a metal-lined hollow glass fiber. *Fusion Sci. Technol.* **2015**, *67*, 547–550. [[CrossRef](#)]
97. Guo, J.J.; Yang, D.W.; Liu, C.H. Raman signal enhancement for gas detection using a hollow core optical fiber. *Spectrosc. Spectr. Anal.* **2016**, *36*, 96–98.
98. Qi, D.; Berger, A.J. Chemical concentration measurement in blood serum and urine samples using liquid-core optical fiber Raman spectroscopy. *Appl. Opt.* **2007**, *46*, 1726–1734. [[CrossRef](#)]
99. Qiao, P.; Wang, X.H.; Gao, S.; Yin, X.; Wang, P. Integration of black phosphorus and hollow-core anti-resonant fiber enables two-order magnitude enhancement of sensitivity for bisphenol A detection. *Biosens. Bioelectron.* **2019**, *149*, 111821. [[CrossRef](#)]
100. Azkune, M.; Frosch, T.; Arrospide, E.; Aldabaldetretu, G.; Bikandi, I.; Zubia, J.; Popp, J.; Frosch, T. Liquid-core microstructured polymer optical fiber as fiber enhanced raman spectroscopy probe for glucose sensing. *J. Lightwave Technol.* **2019**, *37*, 2981–2988. [[CrossRef](#)]